IMPROVEMENT OF GAS SENSING SELECTIVITY OF VANADIUM PENTOXIDE NANO-STRUCTURES TOWARDS SULPHUR DIOXIDE BY GOLD DOPING

By

MOKWENA MICK MOLUKIE

DISSERTATION

Submitted in fulfilment of the requirements for the degree of

MASTER OF SCIENCE

In

PHYSICS

In the

FACULTY OF SCIENCE AND AGRICULTURE

(School of Physical and Mineral Sciences)

At the

University of Limpopo

Supervisor: Dr O. O. Nubi

Co-supervisor: Dr A. A. Akande (University of Sydney, Australia)

2023

Declaration

I declare that the completed work titled “improvement of gas sensing selectivity of vanadium pentoxide nano-structures towards sulphur dioxide by gold doping.” handed in at the University of Limpopo is my own work and all materials used as references have been acknowledged accordingly. To the best of my knowledge this work has never been submitted in any institution for any other degree or assessment.

Mokwena M.M. Date: 10/05/2023

Acknowledgements

I would like to thank the following parties in fulfilment to my MSc:

- ✓ The University of Limpopo for giving me the opportunity to further my studies.
- ✓ My supervisors Dr. O.O. Nubi and Dr A.A. Akande for the exceptional guidance and mentorship towards completing my degree.
- ✓ The Council for Scientific and Industrial Research (CSIR) for the financial assistance towards obtaining my qualification and the centre for Nano-structured materials for allowing us access to their characterisation equipment's.
- ✓ My family for their unyielding support throughout my academic journey.
- ✓ My classmates for their assistance in other concepts similar to our distinct research applications/studies.
- ✓ All individuals that contributed to the completion of my research regardless of how big or small, I appreciate it.

Dedication

This work is dedicated to:

My mother

Shilubane Bonisiwe Beauty

My late father

Mokoena Enos Rasenale

All my siblings

Mokwena Kenneth Andrew

Mokoena Eddie Thony

Mokoena Rabie Jeffrey

Mokoena Lucia Mapule

Mokoena Jackie King

Mokwena Carol Balebogile

Abstract

A facile reflux method was used to synthesise undoped and Au-doped V_2O_5 nanoparticles powder samples at concentrations ranging from 1 wt% to 5 wt%. The prepared samples' structural and optical properties were examined using x-ray diffraction (XRD), scanning electron microscopy (SEM), energy dispersive x-ray spectroscopy (EDS),Brunuaer-Emmett-Teller (BET),ultraviolet-visible spectroscopy (UV-Vis) and Fourier transform infrared spectroscopy (FT-IR). The XRD diffractograms confirmed that the prepared samples have an orthorhombic crystal structure. The lattice parameters of undoped and Au-doped V_2O_5 samples were determined and found to match with those of bulk V_2O_5. The average crystallite size of the undoped and Au-doped V_2O_5 was found to increase at low Au concentrations (1 wt% - 3 wt%) and decrease at high Au concentrations (4 wt% - 5 wt%) due to an increased number of nucleation sites. The SEM images showed morphological changes from spherical to nanorods for undoped and doped V_2O_5 respectively. The elemental composition of the undoped and Au-doped V_2O_5 nanoparticles were confirmed using EDS. The same was done for the 2 wt% Au-doped V_2O_5 sample that was contaminated by mercury (Hg). BET was used to probe the surface area of the undoped and Au-doped V_2O_5 while also confirming that all the samples were mesoporous. The band gap of the undoped and Au-doped V_2O_5 samples were determined from the UV-Vis absorption spectra and found to increase at high Au concentrations. The functional groups present in all prepared samples were investigated using FTIR spectroscopy.

Contents

List of figures

List of tables

Chapter 1: Introduction

1.1. Background

Vanadium is one of the most abundant elements in the Earth's crust and has been observed to exist in a variety of valence states. Vanadium monoxide (VO), vanadium sesquioxide (V_2O_3), vanadium dioxide (VO_2), and vanadium pentoxide (V_2O_5) form part of the most significant oxides of vanadium which exist as single valence oxides in oxidation states V^{2+} to V^{5+} [1, 2, 3]. Nevertheless, the introduction of oxygen vacancies into the higher oxides of vanadium forms vanadium oxides with mixed valence oxides containing more than one oxidation state, such as V_3O_7, V_4O_9 (with oxidation states of V^{5+} and V^{4+}), as well as a series of oxides: V_6O_{11} ,V_7O_{13} and V_8O_{15} (with oxidation states of V^{4+} and V^{3+}) [4, 5]. Two series of phases are formed from the mixing of phases: the Magnéli phase V_nO_{2n-1} and the Wadsley phase V_nO_{2n+1} [1].

The most significant vanadium oxide is vanadium pentoxide and has attracted much attention throughout the years due to its excellent electrical, optical, and magnetic properties. The mineral type of this compound, Shcherbianaite, is amazingly uncommon, quite often found among fumaroles. It is a scentless earthy colored/yellow translucent powder, even though its tone is profound orange when recently precipitated from aqueous solution. V_2O_5 has the four well known structural polymorphs: α-V_2O_5, β-V_2O_5, γ′-V_2O_5, and ε′-V_2O_5 [6]. With α-V_2O_5 being the most stable phase and has lattice parameters of *a* = 1.1512nm, b = 0.3564nm and c = 0.4368nm. At higher temperatures or pressure the α-V_2O_5 phase changes into the other metastable phases [5, 6]. It has a layer-like structure and from a synthetic perspective, V_2O_5 is a fantastic catalyst because of its rich and diverse science that

depends on two factors: the difference of vanadium oxidation states, (ranging from V^{2+} to V^{5+}), and the distinction of oxygen coordination geometries [5].

Vanadium pentoxide is an inorganic n-type semiconducting material with an optical band gap energy of 2.38 eV at room temperature [7]. It is both an amphoteric oxide and an oxidizing agent due to its elevated oxidation state of V^{5+}. It is less toxic compared to most other metal oxides, and has shown great application due to its redox-activity and layered structure. It is the main compound of vanadium from a horticultural perspective, being the fundamental forerunner of vanadium composites and a usually utilized mechanical catalyst [8]. Vanadium pentoxide is a significant business substance for the most part utilised in the steel industries. It is used in ceramics and in the fabrication of superconductive magnets. It is also used as a catalyst in color, paint and stain drying, glass and ink assembling, pesticides, and photographic chemicals [9].

V_2O_5 is most commonly used in lithium-ion batteries as a cathode to improve capacity, voltage (versus the anode material), reversibility, and stability [10, 11, 12]. It is a very good candidate for capacitor applications and can be used as walls in fusion reactors due to its low cost. Further, single phase V_2O_5 is probably the most studied oxide due to ease of synthesis at low cost and high flexibility in versatile device fabrication [13, 14, 15]. A wide range of nano-sized vanadium oxides have been synthesized using sol-gel, solvothermal, pulsed laser deposition, reactive magnetron sputtering to produce nanorods, nanowires, nanotubes, nanobelts and etc [16, 17, 18].

1.2. Problem Statement

Due to the exponential growth of industrial entities and agricultural bodies to upgrade and fit human lives to the standard of the modern world, a lot of prospects have changed for the better in household, medical, transportation and entertainment utilities

[19]. Even though the changes present great improvement to society, they also have drawbacks in the form of air pollutants emitted through various processes. Air pollution has proven to be a worldwide predicament since some studies have found that it can cause about 5 million deaths in a single year [20]. H_2S is an achromic, toxic substance that has a rotten egg-like pungent smell mainly produced from industries, human waste excretions, and the decaying of living organisms [21]. Even at concentrations as low as 10ppm over a period of 8 hrs, H_2S can cause severe health conditions for human lives ranging from simple irritation (sneezing, coughing, etc.) to kidney and lung diseases according to the Occupational Safety and Health and Safety Administration (OSHA) [22]. H_2S exposure from domestic production has recently attracted significant attention worldwide, both for the general public and those who work with hazardous materials [23]. Recent studies have highlighted the threat posed by H_2S poisoning especially from large supply and service-rendering companies in all countries [24]. Current semiconductor metal oxide (SMO) based H_2S gas sensors have shown good selectivity only at temperatures above 500^oC, which leads to harsh operating conditions, instability and high-power consumption. Therefore, the present work aims to produce a sensor that will operate at low temperatures to reduce power consumption, increase stability and repeatability of H_2S gas sensors using gold as a dopant.

1.3. Rationale

Due to their low cost and quick preparation time, SMO materials have been studied substantially as potential gas sensor materials and their portability compared to procedures like gas chromatography and spectrometry [25]. The world of SMOs as gas sensor materials has recently been revolutionised through the contribution of new and novel materials such as vanadium pentoxide (V_2O_5) nanostructures. V_2O_5 has

been found to stand out among the classes of vanadium oxide materials for gas sensing applications due to its exceptional electrical, optical, and magnetic properties as well as its surface adsorption characteristics and catalytic activities. [26]. The material has also been applied as a dopant and catalyst to other SMO for CH_3OH and H_2S gas detection at various concentrations and ambient conditions. However, for a material to be well suitable as a gas sensing element, criteria such as the response ability (rapid response and recovery times) and operating temperature are key requirements [19]. Other important requirements are stability and the ability to select a target molecule during detection (often called selectivity). To realise the above requirements, certain optimisation on the synthesis methods and necessary modifications and doping are needed to alter the intrinsic properties and surface structure of the material. In the work by Modafferi et. al. [27], in order to create vanadium oxide/polyvinyl acetate (V_2O_5/PVAC) fibers, the straightforward sol-gel process was used. The produced V_2O_5 sensor demonstrated exceptional ammonia sensitivity between 200 and 250^oC, with response and recovery durations of 50 and 350 s, respectively. Yildirim et. al. [28] reported that V_2O_5 nanostructures were synthesised using the hydrothermal method at varying deposition times of 4,6,8 and 10 hours in an autoclave at 180^oC. The gas sensing performance of V_2O_5 nanostructure deposited for 6 hours showed better gas detection properties compared to the other V_2O_5 samples at 50 ppm H_2S gas. V_2O_5 sensor had a response of 88% towards H_2S at 145^oC operating temperature with response and recovery times of 1.4s and 1.4s respectively [28]. Studies have shown that doping V_2O_5 with gold (Au) can lower the operating temperature and enhance the selectivity of the sensor towards methane gas which automatically improves the sensitivity as well, due to its distinct electronic structure and high surface to volume ratio. Liang et. al. [29] reported that Au

decorated vanadium oxides were synthesised using the dc magnetron sputtering method. The prepared vanadium oxide samples gas detection properties were tested towards methane (CH_4) gas and showed great response towards CH_4 gas at room temperature. This work sets out to produce a V_2O_5 sensor that would be more selective towards H_2S gas since H_2S gas is harmful to human lives at concentrations as low as 100ppm according to NIOSH. The intended sensor would also operate at low temperatures ranging from room temperature to 150^oC, since current H_2S gas sensors exhibit an undesired characteristic of instability at temperatures above 300^oC and to avoid aggregation of V_2O_5 particles.

1.4. Aims and Objectives

1.4.1. Aim:

The aims of the study were:

1. To investigate the influence of gold (Au) on the structural and optical properties of V_2O_5 nanostructures.

1.4.2. Objectives:

The objectives of the study were to:

i. synthesise the undoped V_2O_5 and V_2O_5 doped with various concentrations of Au using the reflux method.
ii. Investigate the structures of undoped and Au-doped V_2O_5.
iii. Investigate the optical properties of the undoped and Au-doped V_2O_5.

1.5. References

[1] T. K. Le, M. Kang and W. S. Kim, "A review on the optical characterization of V2O5 micro-nanostructures," *Ceramics International,* vol. 45, no. 13, pp. 15781-15798, 2019.

[2] Lenntech, 01 02 2021. [Online]. Available: www.lenntech.com. [Accessed Monday February 2021].

[3] L. K. Ryan, "Vanadium Pentoxide Effects on Lungs," *Encyclopedia of Metalloproteins,* 2013.

[4] S. Surnev, M. G. Ramsey and F. P. Netzer, "Vanadium oxide surface studies," *Progress in Surface Science,* vol. 73, no. 4-8, pp. 117-165, 2003.

[5] S. Beke, "A review of the growth of V2O5 films from 1885 to 2010," *Thin Solid Films,* vol. 519, pp. 1761-1771, 2011.

[6] M. B. Smirnov, E. M. Roginskii, K. S. Smirnov, R. Baddour-Hadjean and J.-P. Pereira-Ramos, "Unraveling the Structure−Raman Spectra Relationships in V2O5 Polymorphs via a Comprehensive Experimental and DFT Study," *Inorganic Chemistry,* vol. 57, pp. 9190-9204, 2018.

[7] M. Al Zoubi, H. K. Fang and F. Endres, "Sol-gel synthesis of vanadium pentoxide nanoparticles in air- and water-soluble ionic liquids," *Journal of material Science,* vol. 44, no. 5, pp. 1363-1373, 2009.

[8] G. Bauer, V. Güther , . H. Hess, A. Otto, O. Roidl, H. Roller, . S. Sattelberger, . S. Köther-Becker and T. Beyer, "Vanadium and Vanadium Compounds," *Ullmann's Encyclopedia of Industrial Chemistry,* 2005.

[9] "National Center for Biotechnology Information," PubChem Compound Summary for CID 14814, Vanadium pentoxide, 8 February 2021. [Online]. Available: https://pubchem.ncbi.nlm.nih.gov/compound/Vanadium-pentoxide.. [Accessed 8 February 2021].

[10] C. Wu and Y. Xie, "Promising vanadium oxide and hydroxidenanostructures: from energy storage to energy saving," *Energy & Environmental Science,* no. 9, 2010.

[11] C. Q. Feng, S. Y. Wang, R. Zeng, Z. P. Guo, K. Konstantinov and H. K. Liu, "Synthesis of spherical porous vanadium pentoxide and its electrochemical properties," *Journal of Power Sources,* vol. 184, no. 2, pp. 485-488, 2008.

[12] C. M. Ly, " Electronic Structure of V2O5 Polymorphs and MxV2O5 Bronzes," Texas A & M University, 2018.

[13] M. Kovendhan, D. P. Joseph, P. Manimuthu, A. Sendilkumar, S. N. Karthick, S. Sambasivam, K. Vijayarangamuthu, H. J. Kim, B. C. Choi, K. Asokan, C. Venkateswaran and R. Mohan, "Prototype electrochromic device and dye sensitized solar cell using spray deposited undoped and ‘Li’ doped V2O5 thin film electrodes," *Current Applied Physics,* vol. 15, no. 5, pp. 622-631, 2015.

[14] I. Pradeep, E. Ranjith Kumar, N. Suriyanaranan, C. Srinivas and N. Venkata Rao, "Structural, optical and electrical properties of pure and Fe doped V2O5

nanoparticles for junction diode fabrications," *Journal of Materials Science: Materials in Electronics,* vol. 29, p. 9840–9853, 2018.

[15] R. T. Rajendra Kumar, B. Karunagaran, V. Senthil kumar, Y. L. Jeyachandran and S. K. Narayandass, "Structrural of V2O5 thin films prepared by vacuum evaporation," *Materials Science in Semiconductor Processing,* vol. 6, no. 5-6, pp. 543-546, 2003.

[16] D. Pham-Cong, K. Ahn, S. W. Hong, S. Y. Jeong, J. H. Choi, C. H. Doh, J. S. Jin, E. D. Jeong and C. R. Cho, "Cathodic performance of V2O5 nanowires and reduced graphene oxide composites for lithium ion batteries," *Current Applied Physics,* vol. 14, no. 2, pp. 215-221, 2014.

[17] C. Niu, J. Li, H. Jin, H. Shi, Y. Zhu, W. Wang and M. Cao, "Self-template processed hierarchical V2O5 nanobelts as cathode for high performance lithium ion battery," *Electrochimica Acta,* vol. 182, no. 10, pp. 621-628, 2015.

[18] R. K. Jain and A. Khanna, "Structural, optical and electrical properties of crystalline V2O5 films deposited by thermal evaporation and effects of temperature on UV–vis and Raman spectra," *Optik,* vol. 144, pp. 271-280, 2017.

[19] K. Wetchakun, T. Samerjai, N. Tamaekong, C. Liewhiran, C. Siriwong, V. Kruefu, A. Wisitsoraat, A. Tuantranont and S. Phanichphant, "Semiconducting metal oxides as sensors for environmentally hazardous gases," *Sensors and Actuators B: Chemical,* vol. 160, p. 580– 591, 2011.

[20] H. Ritchie and M. Roser, Air Pollution, 2017.

[21] X. Hu, Z. Zhu, C. Chen, T. Wen, X. Zhao and L. Xie, "Highly sensitive H2S gas sensors based on Pd-doped CuO nanoflowers with low operating temperature," *Sensors and Actuators B: Chemical,* vol. 253, pp. 809-817, 2017.

[22] A. MacCarley, "Acute and chronic sulphur dioxide (SO2) exposure: an overview of its effects on humans and laboratory animals.," California Polytechnic State University, San Luis Obispo, California, 2013.

[23] P. Pressman, R. Clemens, S. Sahu and A. W. Hayes, "A review of methanol poisoning: a crisis beyond ocular toxicology," in *Cutaneous and Ocular Toxicology*, 3 ed., vol. 39, 2020, pp. 173-179.

[24] MARS Reports, "Real life accidents: Hydrogen sulphide (H2S) gas almost kills crew members on ship," *Marine insight,* 1 November 2013.

[25] N. Joshi, T. Hayasaka, Y. Liu, . H. Liu, O. N. Oliveira Jr and L. Lin , "A review on chemiresistive room temperature gas sensors based on metal oxide nanostructures, graphene and 2D transition metal dichalcogenides," *Microchimica Acta,* pp. 185-213, 2018.

[26] N. K. Nandakumar and E. G. Seebauer, "Low temperature chemical vapor deposition of nanocrystalline V2O5 thin films," *Thin Solid Films,* vol. 519, no. 11, pp. 3663-3668, 2011.

[27] V. Modafferi, G. Panzera, A. Donato, P. L. Antonucci, C. Cannilla, N. Donato, D. Spadaro and G. Neri, "Highly sensitive ammonia resistive sensor based on electrospun V2O5 fibers," *Sensors and Actuators B: Chemical,* vol. 173, no. 1, pp. 61-68, 2012.

[28] A. M. Yildirim, S. T. Yildirim, A. O. Cagirtekin, M. Karademir, I. K. Er, A. Coskun, A. Ates and S. Acar, "The effect of deposition time on the structural, morphological and H2S gas sensing properties of the V2O5 nanostructures deposited by hydrothermal method," *Journal of Materials Science: Materials in Electronics,* vol. 30, pp. 12215-12223, 2019.

[29] J. Liang, J. Liu, N. Li and W. Li, "Magnetron sputtered Au-decorated vanadium oxides composite thin films for methane-sensing properties at room temperature," *Journal of Alloys and Compounds,* vol. 671, pp. 283-290, 2016.

Chapter 2: Literature Review

2.1. Structural Properties of V_2O_5

Semiconducting metal oxides (SMOs) have been widely considered for the fabrication of gas sensors due to their varying morphology, ease of synthesis, large surface area and affinity for microelectronic systems [1]. Several authors claimed that SMO gas sensors could be separated into two simple parts based on the composition of metal oxides involved in the material, which are single and composite metal oxides [2]. The single metal oxides are the likes of WO_3, ZnO, TiO_2, MoO_3, SnO_2, CuO etc., which have been studied over the years for gas detection, however; high operating temperatures and lack of stability remain a challenge [2, 3]. Huge efforts have been made towards doping, decoration, and functionalising of SMOs to enhance their gas sensing capabilities [4, 5]. For instance, Van Hieu et. al. [6] achieved an enhanced sensitivity towards ethanol and liquid petroleum after doping tin oxide with several metal oxides. Nickel oxide nanosheets and graphene foam synthesised using hydrothermal method showed an improved gas sensing performance to CO [7]. Nickle doped zinc oxide nanorods synthesised using a facile solution growth method also showed an improved gas sensing performance to H_2S [8]. Bhati et. al. [9] also achieved an improved sensitivity towards NO_2 after decorating V_2O_5 with reduced graphene oxide (rGO) using the drop cast composite.

Vanadium oxides are a fascinating group of metal oxides especially in the Wadsley phase with V_nO_{2n+1} which can be applied in various fields due to it possessing different oxidation states ranging from V^{2+} to V^{5+} and an interesting V-O coordination chemistry with over 13 nanostructures confirmed through published application studies [10, 11]. The V^{5+} valence state stability prohibits further oxidation which expands its applicability as a catalyst ahead of other valence states such as V^{4+}, V^{3+} and more, but also makes

vanadium oxides a challenging prospect to synthesise since the structures can undergo rearrangement when a certain level of oxygen deficiency is reached [12, 13, 14, 15].

The world of SMOs as gas sensor materials has recently been revolutionised through the contribution of new and novel materials such as V_2O_5 nanostructures. Among the classes of vanadium oxides materials, V_2O_5 has been reported to stand out for gas sensing application not only because of its excellent electrical, high surface to volume ratio, and magnetic properties but also for its surface adsorption characteristics and catalytic activities [16]. V_2O_5 is the most stable compound in the V-O scheme with extremely anisotropic electrical and optical properties owing to its orthorhombic crystal structure as depicted in Figure 2.1.1 and is part of the P_{mmn} space group with lattice parameters of a = 1.1510 nm, b = 0.3563 nm and c = 0.4369 nm [17, 18]. V_2O_5 is also a metal-to-insulator (MTI) transition material with MTI temperature of 260^{o}C and band gap of~2.5 eV [19]. V_2O_5 has a specific conductivity of 0.5 Scm^{-1} at room temperature (RT) and exhibits n-type conductivity in various applications [20]. The layered structure of V_2O_5 is made up of VO_5 square pyramidal shown in Figure 2.1.2, consisting of differently coordinated oxygen with varying bond lengths, vanadyl ($V\text{-}O_1$) with 1.58 Å bond length, bridging ($V\text{-}O_2$) with length 1.77 Å and chain ($V\text{-}O_3$) with length 2.02 Å sharing edges to form a chain-like structure. The V_2O_5 layers allow for intercalation of foreign substances into its valence [21, 22, 23].

Numerous techniques, including hydrothermal [24], chemical spray pyrolysis [25], sputtering methods [26], electrospinning [27], pulsed laser deposition [28], and others, have been reported to produce highly crystalline V_2O_5 nanostructures and thin films for a variety of purposes. Depending on the measurements and settings performed on

the critical parameters of the employed synthesis technique, the morphology of the V_2O_5 nanostructures tends to vary. NH_4VO_3 is mostly preferred as a primary precursor in wet chemical processes for the synthesis of V_2O_5 nanostructures ahead of other precursors such as Na_3VO_4 [29], vanadium foil [30], VCl_3 [31] and etc. Yang et al. [32] reported the fabrication of flower-like V_2O_5 hierarchical structures assembled by nanobelts for 1-butylamine gas detection using a simple hydrothermal approach. 0.117g of NH_4VO_3 and 0.125g of polyvinylpyrrolidone (PVP) were dissolved in 18ml of deionised water under magnetic stirring for 10 minutes at room temperature. 2ml of oxalic acid was then added to the solution under continued stirring for 2hrs until the solution mixture changed color to light green and transferred to a 50ml stainless steel autoclave. The autoclave was kept in an oven for 4hrs at 180^{o}C followed by washing with deionised water and anhydrous alcohol several times before centrifugation and drying at 60^{o}C in air. The flower-like V_2O_5 hierarchical structures were obtained after calcination at 350^{o}C for 2hrs and 400^{o}C for 30 minutes. While physical methods employ pure vanadium metal and ceramic V_2O_5 disc for the preparation of V_2O_5 thin films [28, 33]. Huotari et al. [34] reported the fabrication of vanadium oxide thin films consisting of pure V_2O_5 phase and mixed phases of V_2O_5 and V_7O_{16} believed to be found in vanadium oxide nanotubes (VO_x-NT), A Lambda Physik Compex 201 excimer laser operating at the wavelength of 308 nm was used to deposit vanadium oxide thin films on single crystalline substrate with thickness of 500µm and pulse retention of 5Hz. The PLD process was followed by heat treatment of one of the as-deposited vanadium oxide thin films at 400^{o}C for 1hrs. Post heat treated vanadium oxide sample was found to be V_2O_5 dominant while unheated samples were equally dominated by V_2O_5 and V_7O_{16} and another where dominant V_7O_{16} was found. Stoichiometric defects induced by measurement conditions of PLD procedure on the vanadium oxide thin

films exhibited n-type, p-type conduction along with the presence of V^{5+} and V^{4+} ions due to co-existing V_2O_5 and V_7O_{16} thin films which optimized the gas detection properties of the prepared vanadium oxide thin films towards NO_x and H_2. The nature of V_2O_5 nanostructures synthesised at or below 300^oC deposition temperature tends to be amorphous, and the degree of crystallinity depends on the annealing temperature. Wang et al. [35] also reported the synthesis of spherical V_2O_5 hierarchical structures using the hydrothermal method for trimethylamine detection. Highly pure 0.285g of NH_4VO_3 and 0.9077g of oxalic acid were mixed with 25ml of deionised water under constant stirring until a yellow solution formed, then 3ml of hydrated diammonium was added and stirred further for 1hrs at room temperature until the solution underwent color change to blue. Solution was then transferred to 50ml autoclave and kept in an oven for 6hrs at 180^oC. The dark precipitate was filtered, washed and dried at 60^oC for 12hrs followed by annealing at 400^oC for 2hrs. Stabilizers overcome the Oswald ripening dilemma for experimentalist by controlling the growth of particles, allow solubility and preventing aggregation of nanoparticles.

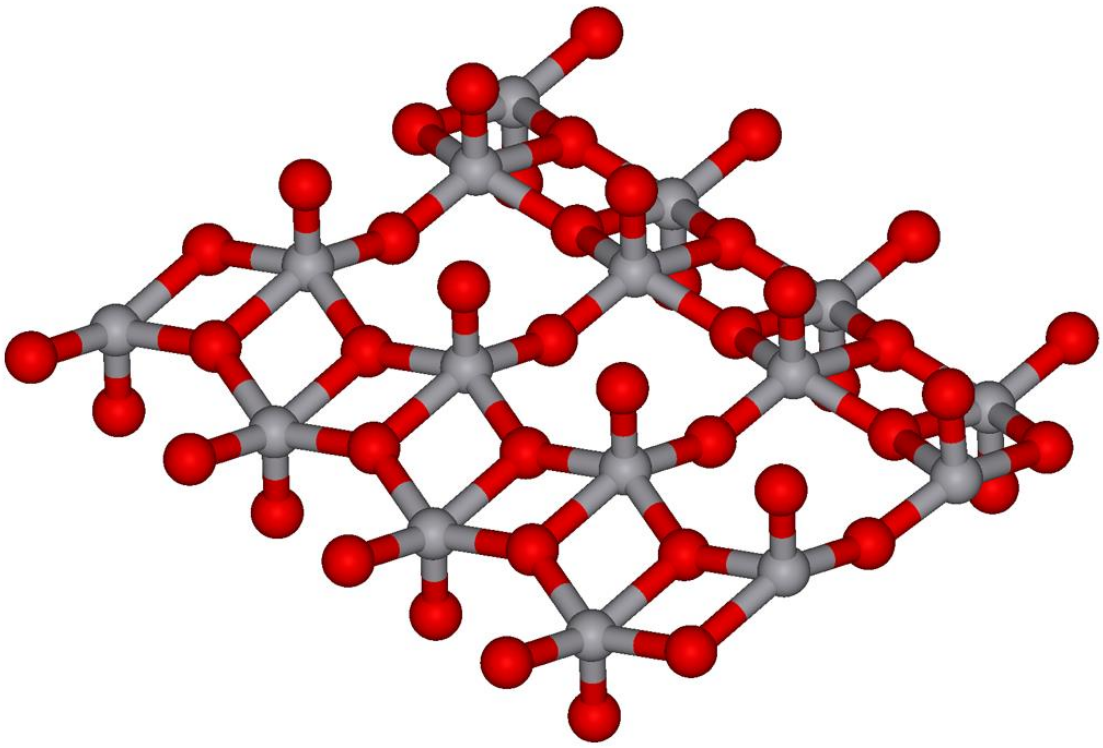

Figure 2.1.1 A depiction of the V_2O_5 layered structure with orthorhombic crystals of red balls (oxygen) and grey balls (vanadium) [36].

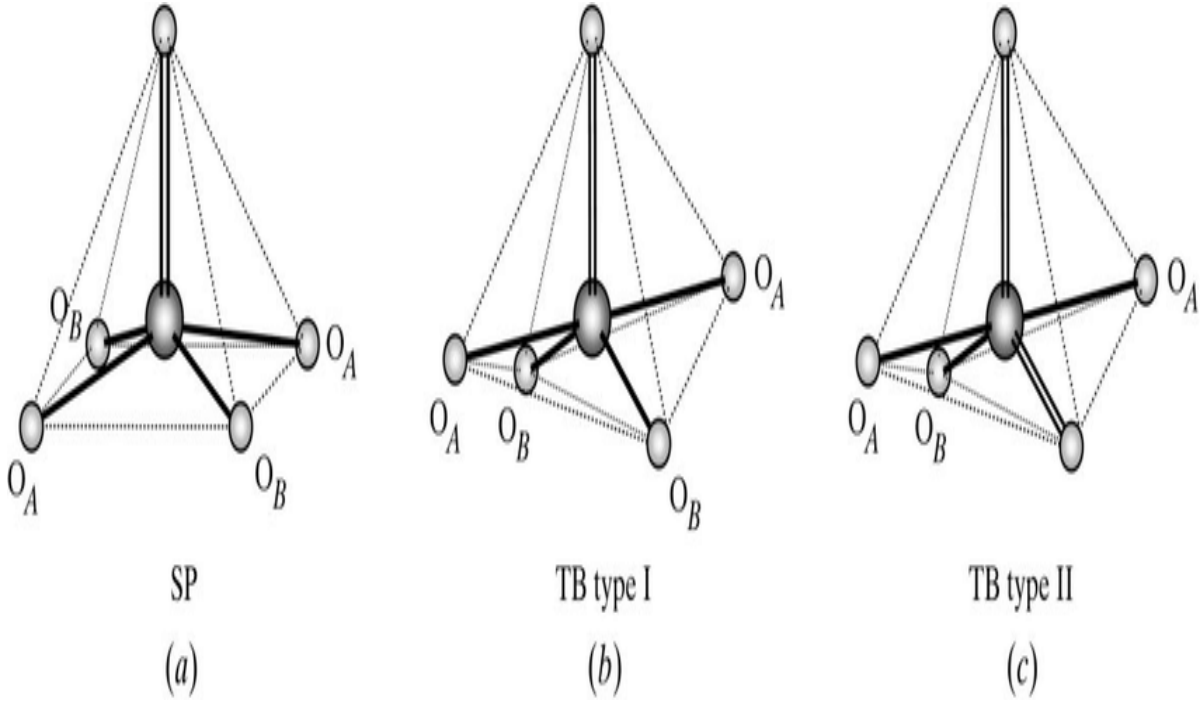

Figure 2.1.2: VO_5 square pyramidal present in the V_2O_5 chain structure [37].

Analysing the XRD pattern provides information about the phase structure, structural orientation, and amorphous state of the material. Govindarajan et al. [38] show V_2O_5 nanostructures calcined at 390^oC exhibit only pure V_2O_5 peaks compared to nanostructures calcined at lower temperatures. Guimaraes et al. [39] reported that bulk V_2O_5 is more crystalline compared to ball milled V_2O_5 for 24hrs because it's purity and single phase nature. Suresh et al. [40] Investigated the structural properties of V_2O_5 and 1%-Zn doped V_2O_5. Zn was observed to shifted V_2O_5 peaks to lower 2θ angles without any Zn peaks visible due to dispersion of Zn^{2+} ion on V_2O_5 crystallites resulting in a reduced crystal size from 35 to 22nm. Also, Kruefu et al. [41] reported the 1.00 mol% Pt-V_2O_5 with V_2O_5 peaks corresponding to orthorhombic crystal phase and Pt peaks corresponding to the cubic phase. A reduced crystallite size was observed for Pt-V_2O_5 compared to V_2O_5 and a shift to higher 2θ angles due to Pt having a bigger atomic radius than V_2O_5. Wang et al. [42] reported the synthesis of Al-free and Al-doped V_2O_5 nanostructures using the chemical vapour deposition at 850^oC and 1.2 x 10^{-1} Torr method on a silicon substrate. Both Al-free and Al-doped V_2O_5 nanostructures exhibit the characteristic orthorhombic V_2O_5 structure, according to the powder XRD study. No unrelated phases, like Al_2O_3 or metallic Al, were found. Al dopant insertion considerably widens the lattice spacing in the a-b plane.

2.2. Optical Properties of V_2O_5

The fabrication methods of V_2O_5 nanostructures are prone to induce defects in the crystal lattice of material. V_2O_5 nanostructures are prone to losing oxygen atoms when subjected to heated environments. This causes the V_2O_5 lattice to dislocate partially and lose oxygen atoms. As a result, the characteristics of the nanostructures are strongly dependent on the synthesis method, leading to the formation of defects or a reduced phase in the resulting layers [43]. The continuous attempts at improving the

physicochemical properties of the V_2O_5 material has produced countless nanostructures with various defects. The electrical structure and surface reactions of vanadium oxide are often affected by oxygen vacancies (V_o) and vanadium vacancies (V_v) known as intrinsic vacancies, which can speed up electron transport and improve electrode functioning [44]. New defects on the electronic structure of V_2O_5 at temperatures above the transition temperature of 257^{o}C reveal the origin of metallic behaviour from the shift of conduction bands when hybrid bonds between the nearest O and V atoms dissociate [45]. Öksüzoğlu et al. [46] reported about pulsed DC reactive sputtered V_2O_5 thin films and the effect of the calcination temperature on the band gap (E_g) of the thin films. The V_2O_5 thin films exhibited a slight increase in the band gap at 180^{o}C due to structural defects leading to high electron (holes) charge concentration and the accumulation of charge barriers, however; at 230^{o}C the band gap decreased to its lowest value due to a change in film structure and an increased crystal size.

When light with a greater energy than the E_g of V_2O_5 interacts with the material, it creates an excitation state that results in the transfer of an electron from the valence band to the conduction band following photon absorption. This phenomenon results in electron-hole pairing [47]. Gavalas et al. [48] reported the aerosol sprayed V_2O_5 thin films deposited at temperatures of 300^{o}C and 400^{o}C using different concentrations of NH_4VO_3 precursor (0.005M, 0.01M and 0.05M). The transmittance of ultraviolet and infrared light by the V_2O_5 thin films was greater at low NH_4VO_3 concentrations and decreased gradually as the precursor concentration increased due to the light absorption coupled with the film thickness of a material. Mane et al. [49] reported chemically spray deposited V_2O_5 thin films with various film thicknesses of 423nm, 559nm, 694nm and 730nm. The V_2O_5 thin films exhibited an increase absorption of UV light as the film thickness was increased due to the high number of atoms residing

in thicker films. Kodu et al. [50] reported graphene functionalised laser ablated V_2O_5 which improved the NH_3 gas response of pristine graphene after UV illumination by 3-fold.

The E_g of the V_2O_5 material can be determined using Plank's relation equation below [51, 52]:

$$E_g = hv_g = \frac{hc}{\lambda} \qquad 2.2.1.1$$

where *c* is the speed of light, (3 x 10^8 $m.s^{-1}$), *h* is the Max Planck's constant (6.63 x 10^{-34} J.s), λ is the cut-off wavelength measured in nm and E_g is the band gap of the material.

Or

Estimated from the tangent line on the Tauc plot represented as the (αhv) versus *hv* graph mathematically represented in the formula [53, 25]:

$$(\alpha hv)^n = A(hv - E_g) \qquad 2.2.1.2$$

Where *hv* is the incident light energy, *A* is a constant value, and *α* is the absorption coefficient. For the indirect band-gap semiconductor, *n* is chosen to be 1/2.

The doping of titanium dioxide (TiO_2), zirconium (Zr) and fluorine (F) into the lattice system or atomic arrangement greatly affects the dynamics of transmittance of light by the V_2O_5 thin films in the visible and infrared region [54]. Suresh et al. [55] reported the thermal decomposition of undoped and Ni-doped V_2O_5 nanoparticles at various concentrations (2, 5 and 7 wt%). The UV-Vis absorption edge of the Ni-doped V_2O_5 exhibited a shift to a higher wavelength of 501nm due to the substitution of Ni^{2+} ions

into the V_2O_5 lattice and significantly reducing the band gap of the material as the concentration of Ni increased. Srilakshmi et al. [56] investigated the effect of doping Ti and Zr on the optical properties of V_2O_5 nanoparticles using the surfactant-micro-emulsion mediated solvothermal method. The band gap of V_2O_5 was significantly reduced from 2.2 eV to 1.96 eV upon doping Ti metal ions due to the presence of oxygen vacancies and titanium ion expanding, however, the band gap increased due to the high concentration of the Zr dopant. Nagaraju et al. [57] reported the chemically sprayed ZnO and V_2O_5/ZnO thins films at various concentrations of V_2O_5 to investigate their effect on the ZnO crystal lattice. The band gap of the ZnO thin films decreased from 3.12eV to 2.97eV as the concentration of V_2O_5 was increased due to minimal amounts of V atoms penetrating the V_2O_5/ZnO thin film layers.

The morphologies, synthesis conditions, crystal size, micro-nano size, phase mixing, and temperature all have an impact on the band structure of the V_2O_5 material which affects the band gap [47].

2.3. Gas Detection Properties of V_2O_5

Despite that the global expansion of industries and agricultural processes have brought great improvements in human lives, industrial growth has been accompanied by the release of various hazardous, ignitable and explosive gases. These include methane gas (CH_4), hydrogen gas (H_2) and hydrogen sulphide (H_2S) and also, other gases like sulphur dioxide (SO_2), nitrogen oxide (NO, NO_2), carbon oxide (CO, CO_2) which become more hazardous when they reach a certain level of concentration called the threshold limit value (TLV) in the atmosphere [58, 2]. SO_2 is a non-flammable, highly toxic greenhouse gas, which might be condensed to a dry fluid with a particular impactful odour [59]. It is used as a precursor for sulphuric acid, refrigerant, reagent and solvent in the laboratory, food preservative/disinfectant, bleaching textiles, climate

engineering and in the biomedical field [60, 61]. Although SO_2 plays a major role in our everyday lives nevertheless, high concentrations of it can cause severe harm to human health and plants [62]. Therefore, the implementation of gas sensitive equipment that can detect such gases before they reach toxic levels (TLV) in the atmosphere is of great importance.

Techniques such as gas chromatography [63], optical gas imaging method [64], quartz crystal microbalance (QCM) [65] and chemi-resistive gas [66] detection approaches have been extensively employed for gas and chemical vapour detection throughout the years. Chemi-resistive gas detectors received preference over the other techniques mentioned above due to low cost, portability, and fast response/sensitivity towards various gases [12]. Gas and chemical sensors play a crucial role in monitoring harmful gases (toxic, explosive, and poisonous) in the atmosphere [12]. Porous material, vapour sensitive polymers and semiconductor metal oxides are the most used material for gas sensing application [67, 68]. Semiconducting metal oxides (SMOs) have been widely considered for the fabrication of gas sensors due to the electrical pathways of the material, varying morphology, ease of synthesis, huge surface area and affinity to microelectronic systems [1]. Leng et al. reported electrospun WO_3 nanofibres for NH_3 detection at 100ppm. The prepared WO_3 nanofibres exhibited a 5.5 response at 500^oC working temperature with response and recovery times of 1 s and 5 s, respectively [69]. A slight change in the valence state of SMO vicinity can alter the catalytic properties of the material [16].

For a material to be well suitable as a gas sensing element, criteria such as response ability, response and recovery times, operating temperature and detection concentration are the key requirement. Other important requirement are stability and

ability to select a target molecule during detection (often called selectivity) [58, 70, 71]. The mathematical representation of the sensor response (S) for n-type material is:

$$S = (R_a - R_g)/R_a \qquad 2.3.1.1$$

Where, R_a is the resistance of the sensor in ambient air and R_g is the resistance of the sensor in the presence of the test gas.

To realise the above-mentioned requirements for the purpose of changing the material's intrinsic properties and surface structure, certain decision needs to be made about the synthesis techniques, measurement of reagents, and doping required.

Generally, semiconductor transition metal oxides are known to exhibit changes in electrical properties when exposed to air because of the adsorbed oxygen molecules which can acquire electrons from conduction band of the SMO surface [58]. The acquisition of electrons would result to an increase in electrical resistance of the SMO.

$$O_{2\ (gas)} \leftrightarrow O_{2\ (adsorbed)} \qquad (2.3.1.2)$$

$$O_{2\ (adsorbed)} + e^- \leftrightarrow O_{2\ (adsorbed)}^- \qquad (2.3.1.3)$$

$$O_{2\ (adsorbed)}^- + e^- \leftrightarrow 2O_{(adsorbed)}^- \qquad (2.3.1.4)$$

$$O_{(adsorbed)}^- + e^- \leftrightarrow O_{(adsorbed)}^{2-} \qquad (2.3.1.5)$$

The ionic oxygen is chemisorbed into O^-, O^-_2, and O^2 as shown in Equations 2.3.1.2 – 2.3.1.5, depending on the temperature of the environment [71, 72, 15]. Electron can be released back to the SMO surface or acquired from SMO depending on whether the SMO is *n* or *p–type* material or whether the analyte gas is a reducing or oxidizing one [58, 73, 74]. V_2O_5 (being n-type material) usually accumulates electrons when exposed to a certain concentration of reducing gas species such as NH_3, CH_4, CO, C_3H_6OH etc. and releases them after the gas is withdrawn. The accumulation of

electrons in the material's conduction band upon gas exposure would lead to a decrease in the resistance of the material.

The following are examples of reaction paths possible when V_2O_5 nanostructures are exposed to reducing gas species in O^- chemisorbed scenario:

$$2NH_3 + 3O^-_{ads} \rightarrow N_2 + 3H_2O + 3e^- \quad (2.3.1.6)$$

$$H_2 + 2O^-_{ads} \rightarrow 4H_2O + 2e^- \quad (2.3.1.7)$$

$$CO + O^-_{ads} \rightarrow CO_2 + e^- \quad (2.3.1.8)$$

$$4H_2 + 2O^-_{ads} \rightarrow 4H_2O + 2e^- \quad (2.3.1.9)$$

$$CH_4 + 4O^-_{ads} \rightarrow 2H_2O + CO_2 + 3e^- \quad (2.3.1.10)$$

$$H_2S + 3O^-_{ads} \rightarrow H_2O + SO_2 + 3e^- \quad (2.3.1.11)$$

In each case, the chemisorbed V_2O_5 surface acquires electrons from the analyte gas and consequently results in a decrease in the electrical resistance of the material. However, when the gas is withdrawn, the material's conduction band evict electrons back to the valence band thereby reverting the resistance of the material back to its original state/value.

On the other hand, the reactions below are examples of reaction paths possible when V_2O_5 nanostructures are exposed to an oxidizing gas species in O^- chemisorbed scenario:

$$NO_{2\ (gas)} + e^- \rightarrow NO^{2-}_{\ (ads)} \quad (2.3.1.12)$$

$$CO_{2\ (gas)} + e^- \rightarrow CO^{2-}_{\ (ads)} \quad (2.3.2.13)$$

Again, in each case, the analyte gas acquires electrons from conduction band of the chemisorbed V_2O_5 surface and consequently this results in an increase in the electrical resistance of the material. However, when the gas is withdrawn, the material's conduction band will gain electron concentration and thereby resulting in a decrease in its electrical resistance [16].

Over the years, many reports which captured synthesis procedures and characterization methods through which determination of properties responsible for enhanced sensing performance have been presented. Table 1 forms a compilation of some records of V_2O_5 based sensor materials coupled with their sensing capabilities. The equations at the bottom of Table 1 show how the response of the material towards several gases (reducing or oxidising) were determined. Table 1 also shows how different V_2O_5 nanostructures of various morphologies can be prepared using solution based, physical vapour deposition and chemical vapour deposition methods.

Table 1: Records of V_2O_5 as a gas sensor material. Responses were determined from the equations $S = R_a/R_g$ { [24] [29] [30] [53] [80] [81] [82] [88] } and $S = (R_g-R_a)/R_a$ { [12] [13] [15] [27] [78] [49] [84] [48] [89]}.

Sensing material	Deposition method	Operating temperature (°C)	Analyte gas	Concentration (ppm)	Sensor response	Response time (s)	Recovery time (s)
V_2O_5 micro/nano tubes	CVD	RT	Humidity	97.2% RH	22	12	25 [13]
V_2O_5 hollow spheres	Solvothermal	370	Triethylamine (TEA)	100	7.3	20	96 [75]
Nanostructured V_2O_5	PLD	350	NH_3	160 ppb	-	-	- [28]
Vanadium oxide/polyvinyl acetate (V_2O_5/PVAC) fibres	Sol gel-based electrospinning	200	NH_3	0.85-8.5	10%	50	350 [27]

V_2O_5 hierarchical structures	Hydrothermal	240	TMA	100	5	5	28 [53]
V_2O_5 thin films	Chemical spray pyrolysis	200	NO_2	100	20,3 %	17	185 [76]
V_2O_5 Ultrathin nanobelts	(EDTA)-medicated hydrothermal method	250	Ethanol	1000	-	-	- [77]
V_2O_5 nanorods	Chemical spray pyrolysis	200	NO_2	100	24.2 %	13	140 [78]
V_2O_5 nanorods	Chemical spray pyrolysis	200	NO_2	100	41%	20	150 [49]
V_2O_5 nanoflakes	-	-	NH_3	100	67.2	14	20 [79]
V_2O_5 hierarchical flower-like structures	Hydrothermal	140	1-butylamine	100	2.6	9	49 [80]
V_2O_5 nanofibres	Chemical spray pyrolysis	RT	Xylene	5-1000	191	80	50 [81]
V_2O_5 hierarchical structures	Hydrothermal	250	NH_3, C_2H_5OH	5	5.3	-	- [82]
V_2O_5 nanobelts	Hydrothermal	20	Ethanol	3-1000	2.9	-	- [82]
V_2O_5 solid-state phase	Pulsed Laser Deposition (PLD)	-	Ammonia, NH_3	40ppb	-	-	- [83]
$V_2O_5.1.6H_2O$ nanostars	Hydrothermal	RT	Helium	300	5.3%	10	9 [84]
Hierarchical V_2O_5 nanoflowers	DC sputtering	100	CH_4	50	8.9%	-	- [12]
V_2O_5 nanorods	Solvothermal method	RT	Ethanol and NH_3	100-500	-	-	- [20]
V_2O_5 flower-like structures	Hydrothermal	200	TMA	1-200	2.17	13	13 [24]

V_2O_5 nanostructures	CVD	400	NH_3	-	-	-	- [18]
V_2O_5 nanourchins	Glycothermal method	150	Acetone	10-1000		200	500 [29]
V_2O_5 nanorods	Oxidation method		Ethanol	500	7.27		[30]
Nanocrystalline V_2O_5 thin films	Plasma focus	275	H_2	1000			[15]
Hollow V_2O_5 nanoassemblies	Polyol approach	RT	H_2	200			[85]
V_2O_5 nanowire microyarns	Electrospinning	330	Ethanol	1000	9.09 %		[86]
V_2O_5 thin films	Rf sputtering		H_2	5-300			[87]
Nanocrystalline V_2O_5 thin films	Chemical spray pyrolysis	250	Ethanol	500	1.80	17	55 [88]
V_2O_5 thin films	Sol gel		Ethanol	100			
V_2O_5 thin films	Aerosol spray pyrolysis	RT	Ozone	5 ppb	29%	120	143 [48]
V_2O_5 thin films	Rf sputtering	326	SO_2	38ppb	0.7		[89]
V_2O_5 nanosheet	DC sputtering	RT	2-propanol	5	2.1	3	10 [90]

In the work by Modafferi et. al. [27] vanadium oxide/polyvinyl acetate (V_2O_5/PVAC) fibres were synthesised using the simple sol-gel method. The prepared V_2O_5 sensor showed tremendous response towards ammonia at 200-250^oC, along with response and recovery times of 50 and 350s respectively. Patil et. al. [91] reported that WO_3, V_2O_5, and WO_3-V_2O_5 nanocomposites thin films were synthesised using the spray pyrolysis method onto a heated glass substrate at 350^oC. The gas sensing performance of pure WO_3, V_2O_5, and different composition of WO_3-V_2O_5 were studied

upon exposure to SO_2 for 500 ppm. WO_3-V_2O_5 was found to have a better sensitivity towards SO_2 at 350^oC operating temperature compared to single WO_3 and V_2O_5 nanocomposites. Studies have shown that doping V_2O_5 with gold (Au) can lower the operating temperature and enhance the selectivity of the sensor which automatically improves the sensitivity as well, due to its distinct electronic structure and high surface to volume ratio. Liang et. al. [92] report that Au decorated vanadium oxides were synthesised using the DC magnetron sputtering method. The prepared vanadium oxide samples' gas detection properties were tested towards methane (CH_4) gas and showed a great response towards CH_4 gas at room temperature.

2.4 References

[1] L. I. Trakhtenberg, G. N. Gerasimov, V. F. Gromov, T. V. Belysheva and O. J. Ilegbusi, "Gas semiconducting sensors based on metal oxide nanocomposites," *Journal of Materials Science Research,* vol. 1, no. 2, 2012.

[2] K. Wu, J. Li and C. Zhang, "Zinc ferrite based gas sensors: A review," *Ceramics International,* vol. 45, no. 9, pp. 11143-11157, 2019.

[3] A. A. Akande, "Gas sensing properties of nanostructured vanadium oxide semiconductors by chemoresistive and optical methods," University of Pretoria, 2017.

[4] G. K. Mani and J. B. B. Rayappan, "A highly selective room temperature ammonia sensor using spray deposited zinc oxide thin film," *Sensors and Actuators B: Chemical,* vol. 183, pp. 459-466, 2013.

[5] O. N. Oliveira Jr, L. Lin, N. Joshi, T. Hayasaka, Y. Liu, H. Liu and O. N. Oliveira Jr, "A review on chemiresistive room temperature gas sensors based on metal oxide nanostructures, graphene and 2D transition metal dichalcogenides," *Microchimica Acta,* vol. 185, no. 213, 2018.

[6] N. Van Hieu, N. A. Phuc Duc, T. Trung, M. Anh Tuan and N. D. Chien, "Gas-sensing properties of tin oxide doped with metal oxides and carbon nanotubes: A competitive sensor for ethanol and petroleum gas," *Sensors and Actuators B: Chemical,* vol. 144, pp. 450-456, 2010.

[7] A. A. Khaleed, A. bello, J. K. Dangbegnon, M. J. Madito, F. U. Ugbo, A. A. Akande, B. P. Dhonge, F. Barzegar, D. Y. Momodu, B. W. Mwakikunga and N. Manyala, "Gas sensing study of hydrothermal reflux synthesized NiO/graphene foam electrode for CO sensing," *Journal of Materials Science,* vol. 52, pp. 2035-2044, 2017.

[8] M. R. Modaferi, R. Rooydell, S. Braham, A. A. Akande, B. W. Mwakikunga and C. Liu, "Enhanced response and selectivity of H2S sensing through controlled Ni doping into ZnO nanorods by using single metal organic precursors," *Sensors and Actuators B,* 2018.

[9] V. S. Bhati, . D. Sheela, B. Roul, R. Raliya, P. Biswas, M. Kumar, M. S. Roy, K. K. Nanda, S. B. Krupanidhi and M. Kumar, "NO2 gas sensing performance enhancement based on reduced graphene oxide decorated V2O5 thin films," 2019.

[10] B. V. Hakala, D. K. Manousou, K. Glazyrin, W. A. Crichton, K. Friese and A. Grzechnik, "Stability of Wadsley-type vanadium oxides V2O5 and V6O13 at high pressures," *Journal of Alloys and Compounds,* vol. 911, p. 164966, 2022.

[11] B. Walls, O. Murtagh, S. I. Bozhko, A. Ionov, A. A. Mazilkin, D. Mullarkey, A. Zhussupbekova, D. A. Shulyatev, K. Zhussupbekov, N. Andreev, N. Tabachkova and I. V. Shvets, "VOx Phase Mixture of Reduced Single Crystalline V2O5: VO2 Resistive Switching," *Materials,* vol. 15, p. 7652, 2022.

[12] V. Mousasamy, G. K. Mani, D. Ponnusamy, K. Tsuchiya, P. R. Reshma, A. K. Prasad and S. Madanagurusamy, "Investigation on CH4 sensing characteristics of hierarchical V2O5 nanoflowers operated at relatively low temperature using

chemiresistive approach," *Analytica Chimica Acta,* vol. 1106, pp. 148-160, 2020.

[13] I. J. Tadeo, R. Parasuraman, S. B. Krupanidhi and A. M. Umarji, Enhanced humidity responsive ultrasonically nebulised V2O5 thin films, Bengaluru: Indian Institute of Science, 2020.

[14] S. Surnev, M. G. Ramsey and F. P. Netzer, "Vanadium oxide surface studies," *Progress in Surface Science,* vol. 73, no. 4-8, pp. 117-165, 2003.

[15] N. Panahl, M. Shirazl and M. Taghi Hosseinnejad, "Fabrication, characterization and hydrogen gas sensing performance of nanostructured V2O5 thin films prepared by plasma focus method," *Journal of Materials Science: Materials in Electronics,* vol. 29, p. 13345–13353, 2018.

[16] L. Tien and Y. Chen, "Influence of growth ambient on the surface and structural properties of vanadium oxide nanorods," *Applied Surface Science,* vol. 274, pp. 64-70, 2013.

[17] N. S. Kumar, M. S. Raman, J. Chandrasekaran, R. Priya, M. Chavali and R. Suresh, "Effect of post-growth annealing on the structural, optical and electrical properties of V2O5 nanorods and its fabrication, characterization of V2O5/p-Si junction diode," *Materials Science in Semiconductor Processing,* vol. 41, pp. 497-507, 2016.

[18] A. A. Akande, T. Mosuang, C. N. Ouma, E. M. Benecha, T. Tesfamichael, K. Roro, A. G. Machatine and B. W. Mwakikunga, "Ammonia gas sensing characteristic of V2O5 nanostructures: A combined experimental and ab initio

density functional theory approach," *Journal of Alloys and Compounds,* vol. 821, p. 153565, 2020.

[19] H. M. R. Gainnetta, C. Calaza, D. G. Lamas, L. Fonseca and L. Fraigi, "Electrical transport properties of V2O5 thin films obtained by thermal annealing of layers grown by RF magnetron sputtering at room temperature," *Thin Solid Films,* vol. 589, pp. 730-734, 2015.

[20] A. Dhayal Raj, T. Pazhanive, P. Suresh Kumar, D. Mangalaraj, D. Nataraj and . N. Ponpandian , "Self assembled V2O5 nanorods for gas sensors," *Current Applied Physics,* vol. 10, pp. 531-537, 2009.

[21] R. Basu, A. K. Prasad, S. Dhara and A. Das, "Role of Vanadyl Oxygen in Understanding Metallic Behavior of V2O5(001) Nanorods," *Journal of Physical Chemistry,* vol. 120, no. 46, p. 26539–26543, 2016.

[22] C. V. Ramana, O. M. Hussain, B. Srinivasulu Naidu and P. J. Reddy, "Spectroscopic characterization of electron-beam evaporated V2O5 thin films," *Thin Solid Films,* vol. 305, no. 1-2, pp. 219-226, 1997.

[23] R. Baddour-Hadjean, V. Golabkan, J. P. Pereira-Ramos, A. Mantoux and D. Lincot, "A Raman study of the lithium insertion process in vanadium pentoxide thin films deposited by atomic layer deposition," *Journal of raman spectroscopy,* vol. 33, no. 8, pp. 631-638, 2002.

[24] D. Meng, J. Si, M. Wang, G. Wang, Y. Shen, X. San and F. Meng, "In-situ growth of V2O5 flower-like structures on ceramic tubes and their trimethylamine sensing properties," *Chinese Chemical Letters,* vol. 31, p. 2133–2136, 2020.

[25] Y. Vijayakumar, G. K. Mani, D. Ponnusamy, P. Shankar, A. J. Kulandaisamy, K. Tsuchiya, J. B. Rayappan and R. M. Ramana, "V2O5 nanofibers: Potential contestant for high performance xylene sensor," *Journal of Alloys and Compounds,* vol. 731, pp. 80-812, 2018.

[26] P. S. Karthikeyan, P. Dhivya, R. P. Deepak and M. Sridharan, "V2O5 thin film for 2-Propanol vapor sensing," *Materials Today: Proceedings,* vol. 3, p. 1510–1516, 2016.

[27] V. Modafferi, G. Panzera, A. Donato, P. L. Antonucci, C. Cannilla, D. Spadaro and G. Neri, "Highly sensitive ammonia resistive sensor based on V2O5 fibres," *Sensors and Actuators B: Chemical,* vol. 163, no. 1, pp. 61-68, 2012.

[28] J. Houtari, R. Bjorklund, J. Lappalainen and A. Lloyd Spetz, "Pulsed Laser Deposited Nanostructured Vanadium Oxide Thin Films Characterized as Ammonia Sensors," *Sensors and Actuators B: Chemical,* vol. 217, pp. 22-29, 2015.

[29] H. Fu, X. Jiang, X. Yang, A. Yu, D. Su and G. Wang, "Glycothermal synthesis of assembled vanadium oxide nanostructures for gas sensing," *Journal of Nanoparticle Research,* vol. 14, p. 871, 2012.

[30] A. H. Shah, Y. Liu and W. Chen, "Synthesis of vanadia nanorod arrays and their novel applications as alco-sensors," *Sensors and Actuators A: Physical,* vol. 264, p. 18–29, 2017.

[31] A. A. Mane, M. P. Suryawanshi, J. H. Kim and A. V. Moholkar, "Fast response of sprayed vanadium pentoxide (V2O5) nanorods towards nitrogen dioxide (NO2) gas detection," *Applied Surface Science,* vol. 403, p. 540–550, 2017.

[32] T. Yang, H. Yu, B. Xiao, Z. Li and M. Zhang, Enhanced 1-butylamine gas sensing characteristics of flower-like V2O5 hierarchical architectures, Changchun: Jilin University, 2017.

[33] C. Imawan, H. Steffes, F. Solzbacher and E. Obermeler, "Structural and gas sensing properties of V2O5-MoO3 thin films for H2 detection," *Sensors and Actuators B,* vol. 77, pp. 346-351, 2001.

[34] J. Huotari, J. Lappalainen, J. Puustinen and A. Lloyd Spetz, "Gas sensing properties of pulsed laser deposited vanadium oxide thin films with various crystal structures," *Sensors and Actuators B: Chemical,* vol. 187, pp. 386-394, 2013.

[35] D. Wang, K. Gu, Q. Zhao, C. Zhai, T. Yang, Q. Lu, J. Zhang and M. Zhang, "Synthesis and trimethylamine sensing properties of spherical V2O5 hierarchical structures," *The Royal Society of Chemistry,* vol. 14, p. 14188, 2018.

[36] M. ,. J. ,. R. ,. M. ,. N. Senthilkumar, "Effect of post-growth annealing on the structural, optical and electrical properties of V2O5 nanorods and its fabrication, characterization of V2O5/p-Si junction diode," p. 2, 2015.

[37] P. Y. Zavalij and M. S. Whittingham, "Structural chemistry of vanadium oxides with open frameworks," *Acta Crystallographica section B,* vol. 55, pp. 627-663, 1999.

[38] D. Govindarajan, V. Uma Shankar and R. Gopalakrishnan, "Supercapacitor behavior and characterization of RGO anchored V2O5," *Journal of Materials Science: Materials in Electronics ,* 2019.

[39] J. L. Guimarães, M. Abbate, S. B. Betim and M. C. Alves, "Preparation and characterization of TiO2 and V2O5 nanoparticles produced by ball-milling," *Journal of Alloys and Compounds,* vol. 352, no. 1-2, pp. 16-20, 2003.

[40] K. Suresh, K. Giribabu, L. Vijayalakshmi, A. Stephen and V. Narayanan, "Visible Light Photocatalytic Property of Zn doped V2O5," *Solid State Physics,* vol. 1447, pp. 351-352, 2012.

[41] V. Kruefu, P. Pookmanee, A. Wisitsoraat and S. Phanichphant, "Gas-sensing Properties of Pt-V2O5 Thin films for Ethanol Detection," *Materials Science and Technology VIII,* vol. 659, pp. 259-263, 2015.

[42] C. Wang, C. Lu, F. Shieu and H. C. Shih, "Structure and Photoluminescence Properties of Thermally Synthesized V2O5 and Al-Doped V2O5 Nanostructures," *Materials,* vol. 14, no. 2, p. 359, 2021.

[43] F. N. Dultsev, L. L. Vasilieva, S. M. Maroshina and L. D. Pokrovsky, "Structural and optical properties of vanadium pentoxide sol–gel films," *Thin Solid Films,* vol. 510, p. 255 – 259, 2006.

[44] Z. Wang, P. Liang, R. Zhang, Z. Liu, W. Li, Z. Pan, H. Yang, X. Shen and J. Wang, "Oxygen-defective V2O5 nanosheets boosting 3D diffusion and reversible storage of zinc ion for aqueous zinc-ion batteries," *Applied Surface Science,* vol. 562, p. 150196, 2021.

[45] R. Basu and S. Dhara, "Spectroscopic study of native defects in the semiconductor to metal phase transition in V2O5 nanostructure," Homi Bhabha National Institute, Tamil Nadu 603102, India, 2018.

[46] R. M. Öksüzoğlu, P. Bilgic, M. Yıldırım and O. Deniz, "Influence ofpost-annealing on electrical, structural and optical properties of vanadium oxide thin films," *Optics & Laser Technology,* vol. 48, pp. 102-109, 2013.

[47] T. K. Le, M. Kang and S. W. Kim, "A Review on the Optical Characterization of V2O5 Micro-1 Nanostructures," *Ceramics International,* vol. 45, no. 13, 2019.

[48] S. Gravlas, E. Ggaoudakis, D. Katerinopoulou, V. Petromichelaki, S. Wight, G. Wotring, E. Apeathitis, G. Kiriakidis and V. Binas, "Vanadium oxide nanostructured thin films prepared by Aerosol Spray Pyrolysis for gas sensing and thermochromic applications," *Materials Science in Semiconductor Processing,* vol. 89, pp. 116-120, 2019.

[49] A. A. Mane and A. V. Moholkar, Effect of film thickness on NO2 gas sensing properties of sprayed orthorhombic nanocrystalline V2O5 thin films, Kolhapur: Shivaji University, 2017.

[50] M. Kodu, A. Berholts, T. Kahro, M. Kook, P. Ritslaid, H. Seemen, T. Avarmaa, H. Alles and R. Jaaniso, "Graphene functionalised by laser-ablated V2O5 for a

highly sensitive NH3 sensor," *Beilstein journal of Nanotechnology,* vol. 8, p. 571–578, 2017.

[51] M. F. Manamela , T. E. Mosuang and B. W. Mwakikunga, "Structural, optical and sensing properties of cobalt and indium doped zinc oxide prepared mechano-chemically," University of Limpopo, Polokwane, 2018.

[52] N. M. Abd-Alghafour, N. M. Ahmed and Z. Hassan, "Fabrication and characterization of V2O5 nanorods based metal–semiconductor–metal photodetector," *Sensors and Actuators A: Physical,* vol. 250, pp. 250-257, 2016.

[53] D. Wang, K. Gu, Q. Zhao, C. Zhai, T. Yang, Q. Lu, J. Zhang and M. Zhang, "Synthesis and trimethylamine sensing properties of spherical V2O5 hierarchical structures," *The Royal Society of Chemistry,* vol. 14, p. 14188, 2018.

[54] E. E. Chain, "Optical properties of vanadium dioxide and vanadium pentoxide thin films," *Applied Optics,* vol. 30, no. 19, pp. 2782-2787, 1991.

[55] R. Suresh, K. Giribabu, R. Manigandan, S. PraveenKumar, S. Munusamy, S. Muthamizh, A. Stephen and V. Narayanan, "New electrochemical sensor based on Ni-doped V2O5 nanoplates modified glassy carbon electrode for selective determination of dopamine at nanomolar level," *Sensors and Actuators B: Chemical,* vol. 202, pp. 440-447, 2014.

[56] P. Srilakshmi, A. Uma Maheswaria, V. Sajeev and M. Sivakumar, "Tuning the optical bandgap of V2O5 nanoparticles by doping transition metal ions," *Materials Today: Proceedings,* vol. 18, p. 1375–1379, 2019.

[57] "Effect of vanadium pentoxide concentration in ZnO/V2O5 nanostructured composite thin films for toluene detection," *Royal Society of Chemistry,* vol. 9, p. 16515, 2019.

[58] Z. Li, H. Li, Z. Wu, M. Wang, J. Luo, H. Torun, P. Hu, C. Yang, M. Grundmann, X. Liu and Y. Fu, "Advances in designs and mechanisms of semiconducting metal oxide nanostructures for high-precision gas sensors operated at room temperature," *Royal Society of Chemistry,* vol. 6, pp. 470-506, 2019.

[59] A. Sathasivan, B. S. Herath, S. T. Senevirathna and G. Kastl, "14 - Dechlorination in Wastewater Treatment Processes," *Current Developments in Biotechnology and Bioengineering,* pp. 359-380, 2017.

[60] G. A. Olah and L. Joachim, "Stable carbonium ions. XLVII. Alkylcarbonium ion formation from alkanes via hydride (alkide) ion abstraction in fluorosulfonic acid-antimony pentafluoride-sulfuryl chlorofluoride solution," *J. Am. Chem. Soc,* vol. 89, no. 18, p. 4739–4744, 1967.

[61] D. Liu, Y. Huang, D. Bu, A. D. Liu, L. Holmberg, Y. Jia, C. Tang, J. Du and H. Jin, "Sulfur dioxide inhibits vascular smooth muscle cell proliferation via suppressing the Erk/MAP kinase pathway mediated by cAMP/PKA signaling," *Cell Death and Disease,* vol. 5, no. 5, p. 1251, 2014.

[62] B. Miller, "Sulfur oxides formation and control," *Fossil Fuel Emissions Control Technologies,* pp. 197-242, 2015.

[63] "Determination of carbon monoxide, methane and carbon dioxide in refinery hydrogen gases and air by gas chromatography," *Journal of Chromatography A,* vol. 989, no. 2, pp. 277-283, 2003.

[64] D. Zimmerle, T. Vaughn, C. Bell, K. Bennett, P. Deshmukh and E. Thoma, "Detection Limits of Optical Gas Imaging for Natural Gas Leak Detection in Realistic Controlled Conditions," *Environmental Science and Technology,* vol. 54, no. 18, p. 11506–11514, 2020.

[65] M. Yang, J. He, X. Hu, C. Yan and Z. Cheng, "CuO Nanostructures As Quartz Crystal Microbalance Sensing Layers for Detection of Trace Hydrogen Cyanide Gas," *Environmental Science and Technology,* vol. 45, no. 14, p. 6088–6094, 2011.

[66] L. Wang, Y. Kang, X. Liu, S. Zhang, W. Huang and S. Wang, "ZnO nanorod gas sensor for ethanol detection," *Sensors and Actuators B: Chemical,* vol. 161, no. 1, pp. 237-243, 2012.

[67] K. Pathakoti, M. Manubolu and H. Hwang, "Nanotechnology Applications for Environmental Industry," *Handbook of Nanomaterials for Industrial Applications,* pp. 894-907, 2018.

[68] Z. M. Rittersma, "Recent achievements in miniaturised humidity sensors—a review of transduction techniques," *Sensors and Actuators A: Physical,* vol. 96, no. 2-3, pp. 196-210, 2002.

[69] J. Leng, X. Xu, N. Lv, H. Fan and T. Zhang, "Synthesis and gas-sensing characteristics of WO3 nanofibers via electrospinning," *Journal of Colloid and Interface Science,* vol. 356, pp. 54-57, 2011.

[70] Z. Yuan, R. Li, F. Meng, J. Zhang , K. Zuo and E. Han, "Approaches to Enhancing Gas Sensing Properties: A Review," *Sensors ,* vol. 19, no. 7, p. 1495, 2019.

[71] F. Sarf, "Synthesis of Metal Oxide Semiconductor Nanostructures for Gas Sensors," in *Gas sensors*, King Abdulaziz University, 2020, p. 168.

[72] M. Takata, D. Tsubone and H. Yanagida, "Dependence of Electrical Conductivity of ZnO on Degree of Sintering," *Journal of the American Ceramic Society,* vol. 59, no. 1-2, pp. 4-8, 1976.

[73] D. Nunes, A. Pimentel, A. Gonçalves, S. Pereira, R. Branquinho, P. Barquinha, E. Fortunato and R. Martins, "Metal oxides nanostructures for sensor applications," *Semiconductor Science and Technology,* vol. 34, no. 4, 2019.

[74] A. Mirzaei and G. Neri, "Microwave-assisted synthesis of metal oxide nanostructures for gas sensing applications: A review," *Sensors and Actuators B: Chemical,* vol. 237, pp. 749-775, 2016.

[75] M. Wu, X. Zhang, S. Gao, Z. Rong, Y. Xu, H. Zhao and L. Huo, "Construction of monodisperse vanadium pentoxide hollow spheres via a facile route and triethylamine sensing property," *Crystal Engineering Community,* vol. 15, no. 46, pp. 10123-10131, 2013.

[76] A. A. Mane, P. S. Maldar, S. H. Dabhole, S. A. Nikam and A. V. Moholkar, "Effect of substrate temperature on physicochemical and gas sensing properties of sprayed orthorhombic V2O5 thin films," *Measurement,* vol. 131, pp. 223-234, 2019.

[77] Y. Qin, L. Zhao and M. Cui, "Ultrathin vanadium pentoxide nanobelt for ethanol-sensing applications: Experimental and ab initio study," *Journal of Alloys and Compounds,* vol. 735, pp. 1480-1487, 2018.

[78] A. A. Mane, M. P. Suryawanshi, J. H. Kim and A. V. Moholkar, "Fast response of sprayed vanadium pentoxide (V2O5) nanorods towards nitrogen dioxide (NO2) gas detection," *Applied Surface Science,* vol. 403, pp. 540-550, 2017.

[79] H. Yin, C. Song, H. Shao, Y. Li, H. Deng, Q. Ma and K. Yu, "Self-Assembled Vanadium Oxide Nanoflakes for p-Type Ammonia Sensors at Room Temperature," *Nanomaterials (Basel),* vol. 3, no. 9, p. 317, 2019.

[80] T. Yang, H. Yu, B. Xiao, Z. Li and M. Zhang, Enhanced 1-butylamine gas sensing characteristics of flower-like V2O5 hierarchical architectures, Changchun: Jilin University, 2017.

[81] Y. Vijayakumar, G. K. Mani, D. Ponnusamy, P. Shankar, A. J. Kulandaisamy, K. Tsuchiya, J. B. B. Rayappan and M. V. Ramana Reddy, "V2O5 nanofibers: Potential contestant for high performance xylene sensor," *Journal of Alloys and Compounds,* vol. 731, pp. 805-812, 2018.

[82] Y. Qin, G. Fan, K. Liu and M. Hu, "Vanadium pentoxide hierarchical structure networks for high performance ethanol gas sensor with dual working

temperature characteristic," *Sensors and Actuators B: Chemical,* vol. 190, pp. 141-148, 2014.

[83] J. Huotari, J. Lappalainen, J. Eriksson, R. Bjorklund, E. Heinonen, I. Miinalainen, J. Puustinen and A. Lloyd Spetz, "Synthesis of nanostructured solid-state phases of V7O16 and V2O5 compounds for ppb-level detection of ammonia," *Journal of Alloys and Compounds,* vol. 675, pp. 433-440, 2016.

[84] P. S. Chauhan and S. Bhattacharya, "Highly sensitive V2O5·1.6H2O nanostructures for sensing of helium gas at room temperature," *Materials Letters,* vol. 217, pp. 83-87, 2018.

[85] Y. Wang, W. Whang and C. Chen, "Hollow V2O5 Nanoassemblies for High-Performance Room-Temperature Hydrogen Sensors," *ACS Applied Materials & Interfaces,* vol. 7, no. 16, pp. 8480-8487, 2015.

[86] W. Jin, S. Yan, L. An, W. Chen, S. Yang, C. Zhao and Y. Dai., "Enhancement of ethanol gas sensing response based on ordered V2O5 nanowire microyarns," *Sensors and Actuators B :Chemical,* vol. 206, pp. 284-290, 2015.

[87] K. Schneider, M. Lubecka and A. Czapla, "V2O5 thin films for gas sensor applications," *Sensors and Actuators B: Chemical,* vol. 236, pp. 970-977, 2016.

[88] M. Abbasi, S. M. Rozati, R. Irani and S. Beke, "Synthesis and gas sensing behavior of nanostructured V2O5 thin films prepared by spray pyrolysis," *Materials Science in Semiconductor Processing,* vol. 29, pp. 132-138, 2015.

[89] C. S. Prajapati and N. Bhat, "Growth optimization, morphological, electrical and sensing characterization of V2O5 films for SO2 sensor chip," in *IEEE Sensors*, Bangalore, India, 2018.

[90] P. S. Karthikeyan, P. Dhivya, R. P. Deepak and M. Sridharan, "V2O5 thin film for 2-Propanol vapor sensing," *Materials Today: Proceedings,* vol. 3, p. 1510–1516, 2016.

[91] J. M. Patil, S. B. Patil, R. H. Bari and A. N. Sonar, "SO2 sensing performance of chemically sprayed WO3-V2O5 nanocomposites thin films," *International Journal of Chemical Concepts,* vol. 2, no. 1, pp. 12-23, 2016.

[92] J. Liang, J. Liu, N. Li and W. Li, "Magnetron sputtered Au-decorated vanadium oxides composite thin films for methane-sensing properties at room temperature," *Journal of Alloys and Compounds,* vol. 671, pp. 283-290, 2016.

Chapter 3: Experimental Procedure and Characterisation Techniques

3.1. Sample Synthesis

3.1.1. The Reflux Method

Refluxing is technically the recapture of the condensed solvent steam in the same medium/container in which it is heated, and the concentration of the reactants is almost constant. The vertical stance of the condenser makes the reflux method distinct from distillation as depicted in Figure 3.1.1. The organic reflux reaction occurs slower at ambient temperature, and increasing temperature accelerates the reaction. Reflux reactions can help avoid the loss of solvents caused by vaporisation in open reactions and avoid explosions in closed vessel reactions during heating (pressure accumulation). Reflux occurs under extreme heat and constant cooling of the condenser, which prevents the reaction vapour from entering the atmosphere. When reflux begins at the bottom of the condenser, the time of reflux is recorded to ensure accuracy under a strict schedule. This method requires a good solvent that can dissolve a reagent but is immiscible to solute and boil at a high enough temperature for the reaction to proceed rapidly or to reach the boiling point of the solvent. The container is half-filled with solution at least before reflux. Boiling stones or stirring bars are used to prevent bumping in solution. Bumping occurs as a violent eruption of large bubbles when a solution is kept under extreme heat [1]. Stirring while refluxing also influences the structural properties of the end product [2]. *In the condensation setup,* the heat source is adjusted so that the condensed vapour ring is around the middle point of the condenser. If the vapour ring is closer to the open edge of the condenser, the solution can be vaporised into the atmosphere and when the vapour ring is around the bottom of the condenser reflux may occur after long periods of time. The reflux method can produce nanostructures of approximately 5-30nm in diameter [3].

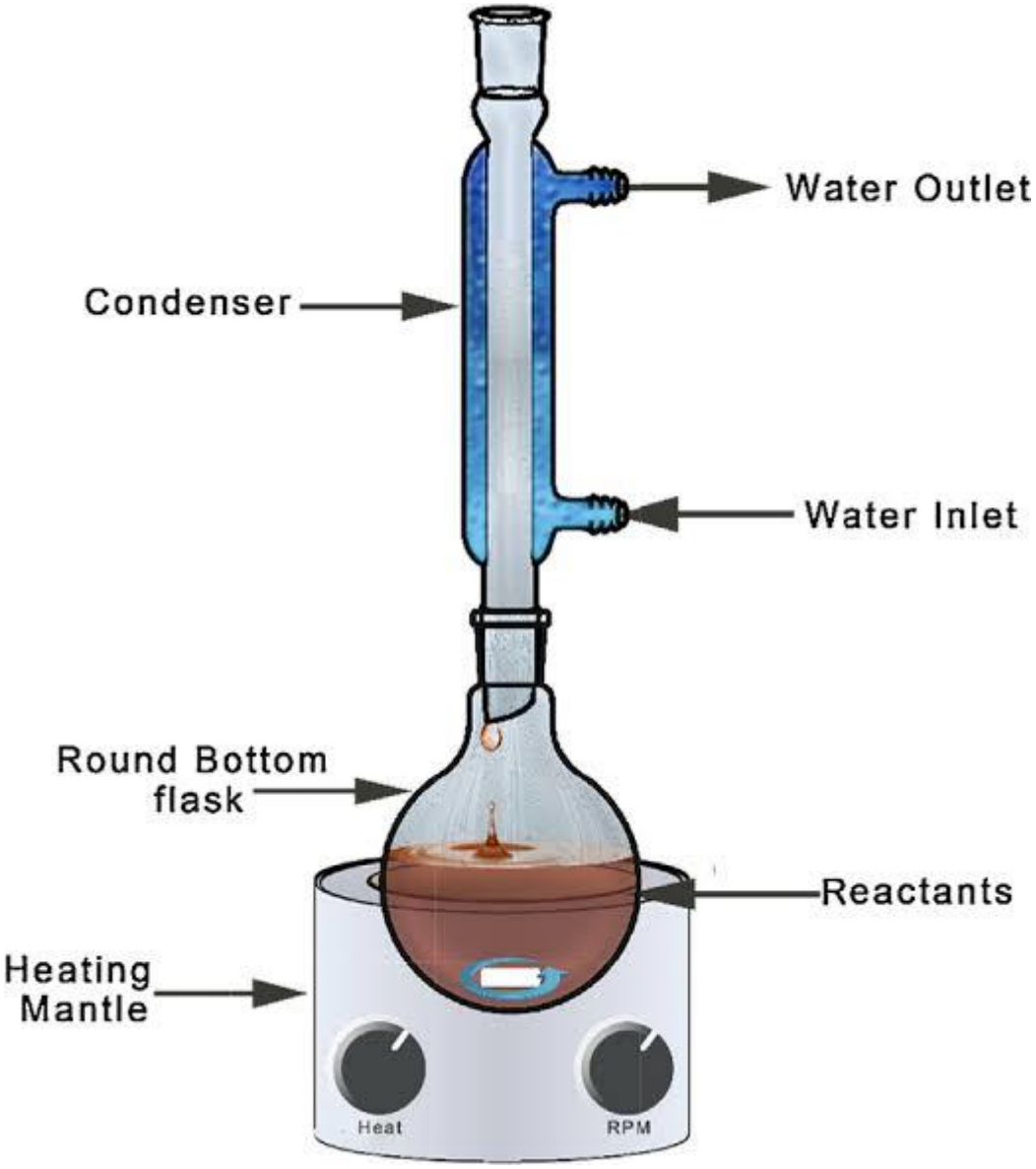

Figure 3.1.1: Depiction of the reflux condensation setup

3.1.2. Procedure

A solution of *NH_4VO_3 (*ammonium metavanadate, 99.0% pure) and $HAuCl_4$ (gold chloride (III) solution, 99.99% pure), purchased from Sigma-Aldrich, were used as precursors without further purification. *2 g of NH_4VO_3 were dissolved in 50 mL ethylene glycol in a glass container and stirred at 70^oC until a bright yellow sol was formed.* The $HAuCl_4$ was added in drops to the solution with continuous stirring. The yellow sol was

then transferred to a reflux condensation unit, with continued stirring, and kept for 2 hrs until dark blue vanadyl glycolate (VEG) precipitates formed. The filtered VEG precipitates were collected through filtering, washed with ethanol several times and dried in a carbolite oven ELF 11/68 model for 8 hrs. This was followed by calcination at 300^{o}C for 3 hrs in air.

3.2. Characterisation Techniques

The kinetic, chemical, optical, and morphological properties of the synthesised samples were analysed using common classification techniques such as X-ray Diffraction (XRD), fourier transform infrared spectroscopy (FT-IR), scanning electron microscopy (SEM), energy dispersive x-ray spectroscopy (EDS) ultraviolet visible spectrometry (UV-Vis), Brunauer, Emmett and Teller (BET).

3.2.1. X-Ray Diffraction

X-ray diffraction is usually used to identify material structure and crystallinity. Most crystalline materials possess atoms situated periodically forming patterns known as unit cells. The distance between these planes is comparable to the wavelength of X-rays. The X-ray photons are dispersed when entering materials due to electron clouds surrounding atoms. The constructive interference from X-rays is produced by the lattice plane periodicity, and the distribution's intensity is defined at a 2θ angle [4]. The XRD experiment was performed using PANalytical X'Pert PRO PW3064/60 X-Ray Diffractometer equipment with copper (Cu) $K\alpha_1$ monochromatic source of radiation through a fixed divergent slit of 0.38mm in diameter. The measurement was done at a voltage of 45 kV, 40mA current and ran between 5^{o} to 60^{o} angle with 0.02^{o} step.

XRD data allows the determination of the d_{hkl} spacing from the diffraction peaks since Bragg's law is satisfied and is expressed mathematically by equation 3.2.1.1 below:

$$n\lambda = 2dsin\theta \qquad 3.2.1.1$$

where *n* represents a number showing the sequence of diffraction, λ is the wavelength of x-rays, *d* is the separation between atom planes that create diffraction peaks and *θ* represent the angle at which x-rays are diffracted. Figure 3.2.1.1 below depicts an instance where parallel incident x-rays are diffracted from a crystal surface at an angle *θ* resulting constructive interference when Bragg's law requirements are met.

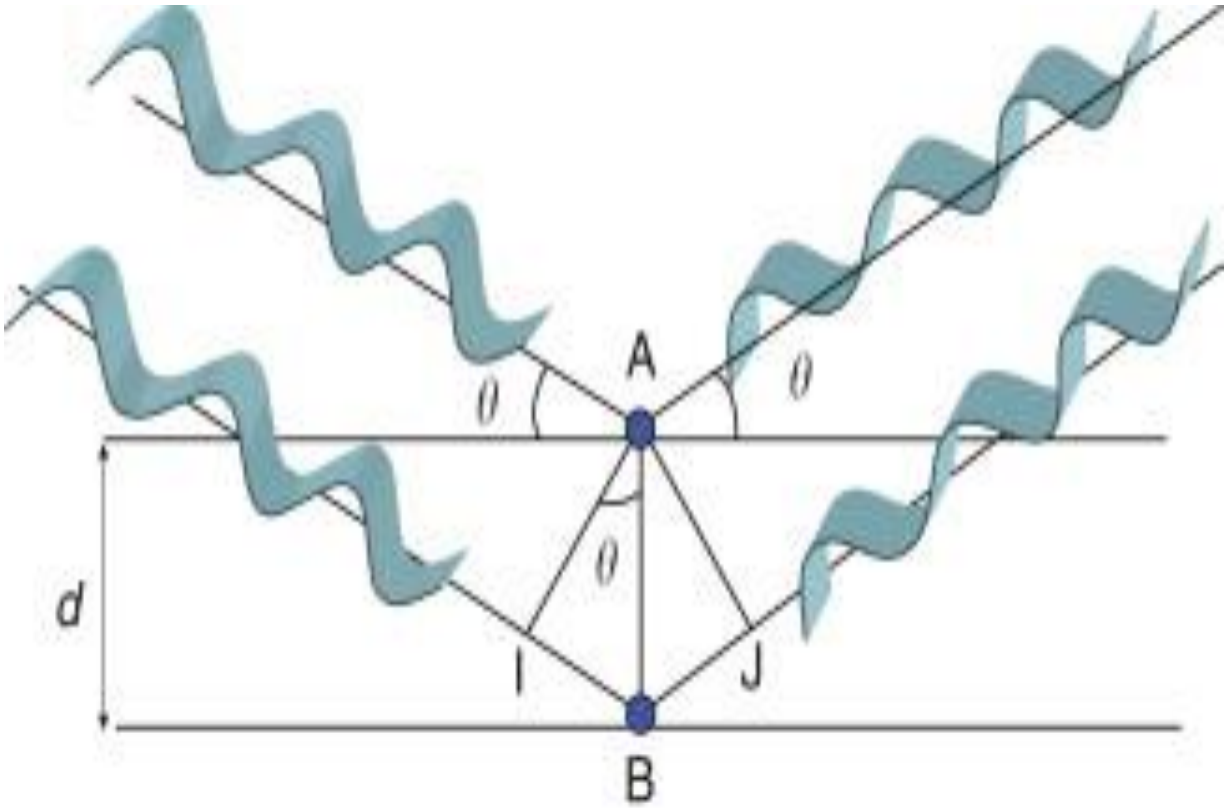

Figure 3.2.1.1: Schematic diagram of the instance Bragg's condition holds [5].

Debye Scherrer's equation, as expressed below, was used to calculate the crystallite size, *D* [6]:

$$D = \frac{k\lambda}{\beta \sin\theta} \qquad 3.3.1.2$$

where k refers to the form of a particle with a magnitude of 0.9, β the peak's full width at its half-maximum (FWHM) in nanometers (nm) and the Bragg's angle θ. The lattice constants *a*, *b* and *c* for an orthorhombic crystal structure are determined using the following formula:

$$\frac{1}{d^2} = \frac{h^2}{a^2} + \frac{k^2}{b^2} + \frac{l^2}{c^2} \qquad 3.2.1.3$$

where $a \neq b \neq c$ and the angle (θ) between lattice constants is 90^o.

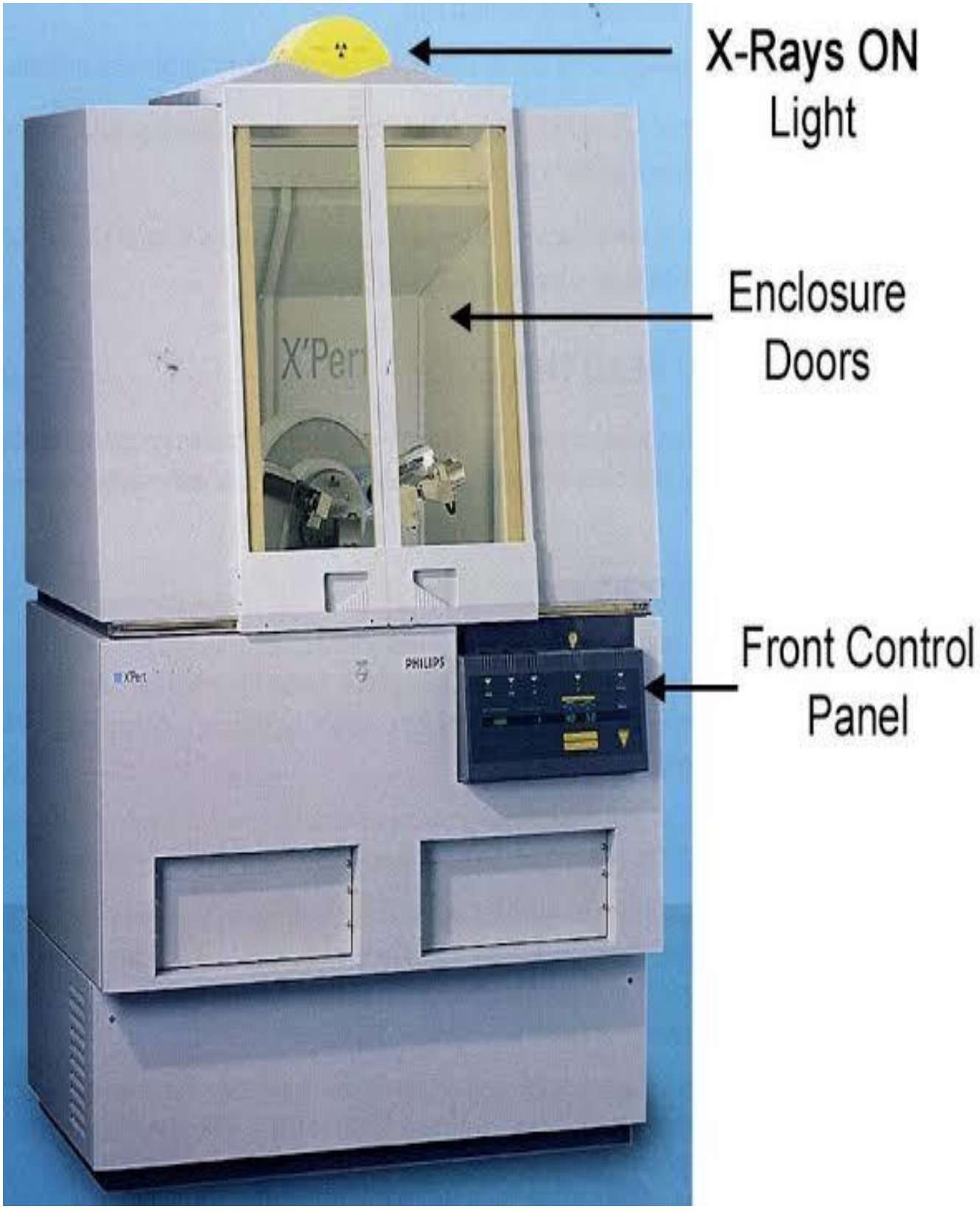

Figure 3.2.1.2: PaNalytical X'Pert Pro diffractometer.

Figure 3.2.1.2 depicts the image of the panalytical x'pert pro diffractometer used to conduct the XRD experiment. Six samples of pure V_2O_5 and Au doped V_2O_5 at concentrations ranging from 1% to 5% were examined for their crystallinity using incident radiation of 1.5406 Á. The XRD data was collected by scanning within the range 9^o to 60^o with a 0.02^o scan step.

3.2.2. Scanning Electron Microscopy (SEM)

SEM is a microscope used to produce images using electrons from an electron gun instead of visible light. The wavelength of light determines an optical microscope's resolution; however, electrons have a shorter wavelength than visible light [7]. The anode, which also controls the accelerating voltage anode, polarizes the electron beam [6]. The electron detector is sensitive to electrons. When an electron beam hits a sample, some electrons are absorbed, some are backscattered, and some are ejected from the sample as secondary electrons. A charge build up may occur if the number of ejected electrons is not equivalent to the number of incident electrons from electron beam. The charge build up may affect the quality of the resulting image, however coating the sample with a thin metal layer prevents the occurrence of charge build up. The SEM image is taken from the collection of secondary electrons since they contain information on surface features of the sample. The reflection of incident electrons that results in the emission of backscattered electrons to create an image. SEM produces 3D images which help in determining the length and width from various morphologies of nanostructures. The scale on the bottom right corner of the images shows the resolution level of the image which can be as low as 1nm or as high as 2 mm for SEM images [7, 8]. The operating principle of SEM is depicted in Figure 3.2.2.1.

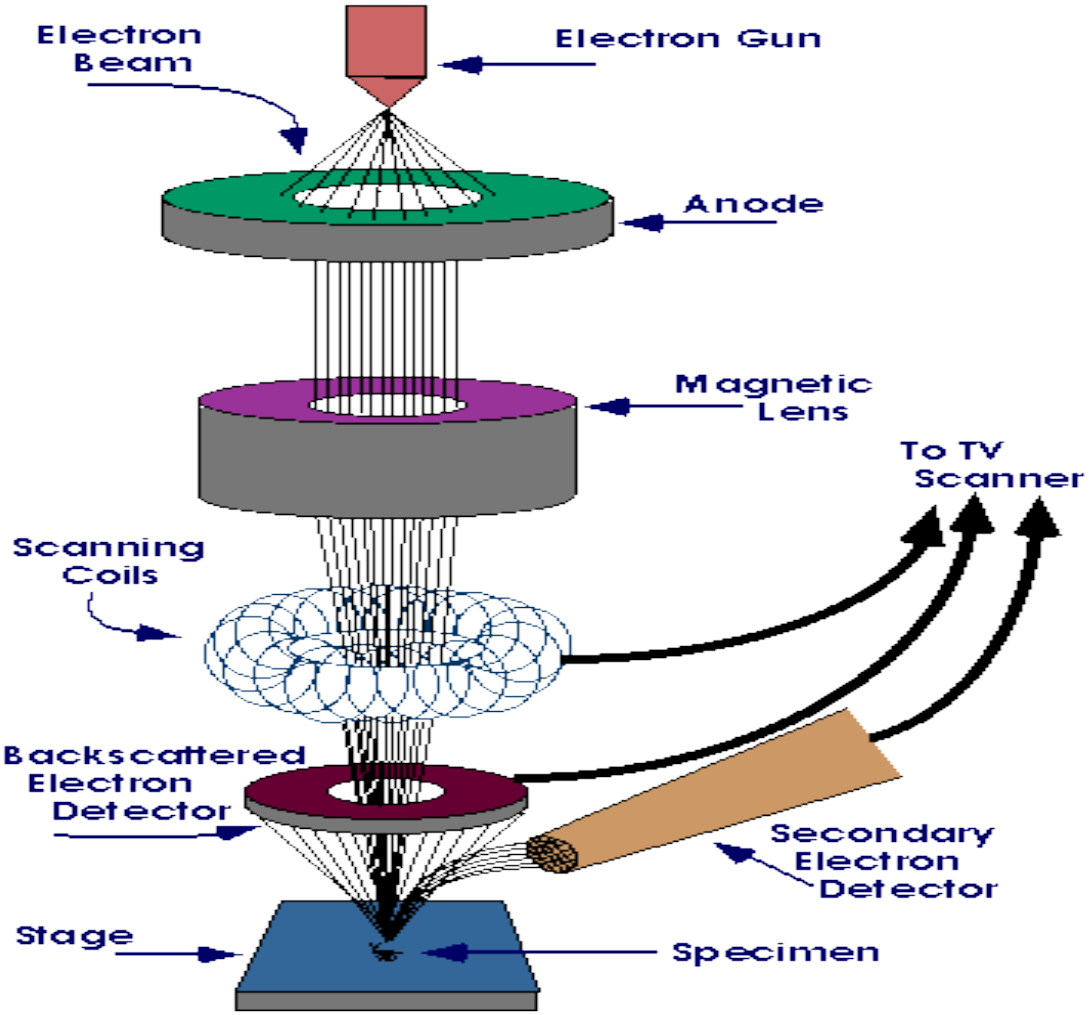

Figure 3.2.2.1: The working principle of SEM [9].

The FEI Quanta 400 FEG-ESEM equipment was used to examine the morphological features of the as-calcined V_2O_5 nanoparticles. The samples were coated with carbon (C) for the SEM images taken using backscattered electron (BSE) and both the in chamber, and inlens secondary electron detectors. The samples were very fine hence the imaging occurred at 15000x and 7000x magnification at scales of 2µm and 3µm respectively.

3.2.3. Energy Dispersive X-Ray Spectroscopy (EDS)

A technique for ascertaining the elemental makeup of solid surfaces is energy dispersive spectroscopy (EDS). The electrons in the target atoms are ejected from their inner shells when a sample is hit with a beam of high-energy electrons, leaving an electron vacancy. In a subsequent transition that releases energy in the form of X-rays, the electrons on the higher energy levels are moved to the inner shell. Each periodic table element has a different electron arrangement, which affects its atomic energy levels. The resulting X-rays are therefore unique to each element. The elemental composition of a sample can be determined by measuring the distinctive X-ray energy and intensity emitted by each element. The excitation source (electron beam or X-ray beam), the X-ray detector, the pulse processor, and the analyser are the four fundamental parts of an EDS device. X-rays are transformed into electric impulses by the X-ray detector.

The analyser processes and displays the data after processing the signals that the pulse processor has detected. The resulting spectrum shows the relationship between the X-ray intensity and energy (in keV). Since the X-ray intensity typically declines as one moves from heavier to lighter elements, the accuracy of EDS is dependent on the precision of the x-ray intensity measurement.

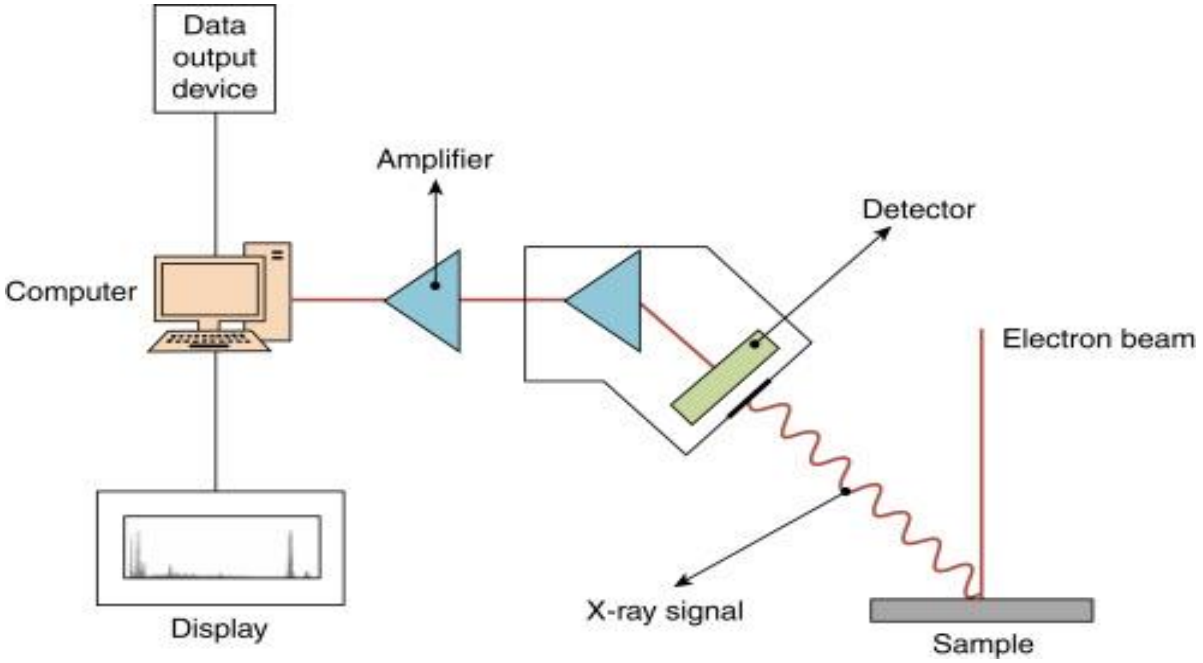

Figure 3.2.3.1: Schematic of an EDS spectroscopy [10].

3.2.4. Brunuaer-Emmett-Teller (BET)

Brunuaer-Emmett-Teller (BET) is a common technique for investigating the gas adsorption, specific surface area and porosity of a solid-state material. It is a development of the Langmiur theory, according to which gaseous molecules adhere to a surface of a substance in a manner similar to how solid-state molecules do, instead of bouncing off of it [11]. Although this method is frequently used for most materials, it is most accurate for materials having a Type II or Type IV isotherm and a high enough level of surface to gas contact. The BET hypothesis might not apply to materials with other types of isotherms for a variety of reasons, thus care is taken. Nonporous or microporous (pore magnitude <2 nm) nanoparticles have Type II isotherms, whereas mesoporous (pore magnitude: 2 - 50 nm) nanoparticles have Type IV isotherms, where adsorption occurs with multilayers followed by capillary condensation at relative pressures (P/P_o) higher than 0.2 [4]. Van der Waal forces, for

example, are weak forces that enable physisorption on a surface because they have low enthalpies approximated around 50 KJ/mol or lower, which prevent the formation of chemical bonds between the adsorbent and adsorbate. N_2 in liquid phase is common for investigation the adsorption and desorption for mesoporous materials. The surface area is determined by using the BET equation expressed as follows:

$$\frac{1}{v[\frac{\mathrm{Po}}{P}-1]} = \frac{1}{C\mathrm{Vm}} + \frac{C-1}{C\mathrm{Vm}} \left(\frac{P}{\mathrm{Po}}\right) \qquad 3.2.4.1[11]$$

where P and P_o represent the adsorbate's equilibrium and saturation pressures at the adsorption temperature. V_m is the monolayer capacity which is the volume of gas at standard temperature and pressure (STP). C is the BET constant and v is the amount of adsorbed gas at a given relative pressure. A plot of $1/v[\frac{\mathrm{Po}}{P} - 1]$ vs P/P_o yields a linear function graph in the range of 0.05 to 0.30 relative pressure.

The intercept "I" and slope "S" of the of the BET plot are:

$S = \frac{C-1}{C\mathrm{Vm}}$ and $I = \frac{1}{C\mathrm{Vm}}$, the monolayer gas capacity can be represented as follows upon rearranging S and I:

$$V_m = \frac{1}{S+1}$$

The specific surface area S_{BET} is thus:

$$S_{BET} = \frac{\mathrm{Vm\ x\ Na\ x\ A}}{V} \qquad 3.2.4.2$$

where N_a is Avogadro's constant, A is the cross-sectional area of adsorbed gas and V is the molar volume STP. Hysteresis occurs due to the pore network of a nano-porous material and its thermodynamic properties. The adsorption and desorption processes exhibited by the four types of Hysteresis (H1 to H4) reveal the nature of pores

possessed by a material [11, 12]. Figure 3.2.4.1 shows the schematic of BET analyses.

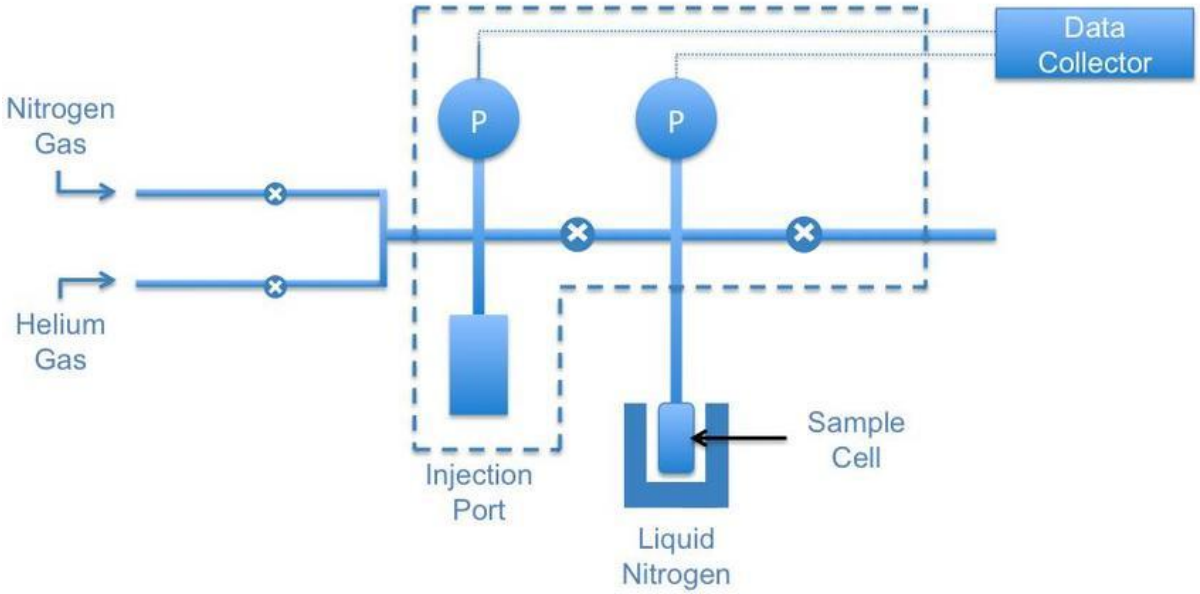

Figure 3.2.4.1: Schematic of BET surface analyser [13].

The Tristar II equipment manufactured by micromeritics-USA was used to conduct the BET experiment. The Au doped V_2O_5 samples were degassed at 120^oC for 2 hrs. The BET surface area, pore size and volume were measured using nitrogen as an adsorbent at 77K.

3.2.5. Ultraviolet-Visible Spectroscopy (UV-Vis)

The optical spectroscopy performed by the UV-Vis spectrophotometer is a technique for analysing the interaction between light and an experimental sample. UV-Vis spectroscopy can be used to determine a sample's optical properties, which includes the reflectance, absorbance, and transmittance of light by the sample [14]. When UV radiation is applied to a sample, it causes the molecules to transition from their low energy state to a high energy state as a result of absorbing energy from the UV radiation source. Thus, an absorption spectrum results from the surplus radiation passed through the sample as an excitation spectrum of molecules that has taken

place within the wavelength region of 190 to 900nm. The UV-Vis light source produces light from two different regions of the spectrum; however, polarisation occurs in the monochromator to allow only light with a single wavelength to interact with the sample [15, 16]. The schematic of the working principle of the UV-Vis spectroscopy is depicted on figure 3.2.5.1. Perkin Elmer UV-Vis spectrophotometer SP-UV 500 was used to conduct the UV-Vis experiment.

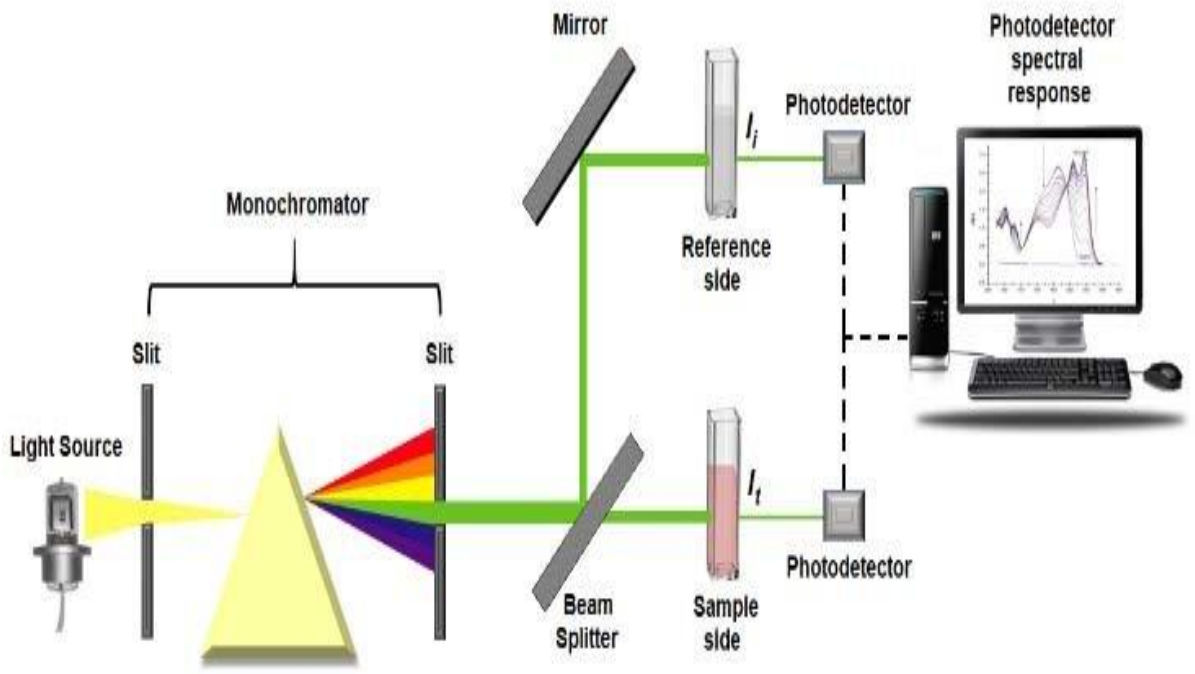

Figure 3.2.5.1: Schematic of UV-Vis process for data analysis [17].

The V_2O_5 samples were dissolved in distilled water solvent which was also used as a blank to run the background to subtract spectrum by excitation of the solvent.

3.2.6. Fourier Transform Infrared Spectroscopy (FT-IR)

FT-IR spectroscopy is a method for analysing the chemical make-up of organic materials, including liquids and solids. The procedure provides graphic information that

is unique to a particular material as a fingerprint that contains the chemical constituents of the material [18]. The sample is subjected to infrared light, which is repeated at several frequency ranges. While some wavelengths of light in the visible spectrum pass through the sample unaltered, others are absorbed by the sample causing molecular vibrations. The system detects the transmitted energies and present the data collected graphically as a plot of intensity against wavenumber (cm^{-1}). The sample fingerprint region is the area with wavenumbers between 0 and 1500 cm^{-1}, and the location, height, and shape of the peaks on the plot indicate the presence of particular chemical bonds in the sample. Figure 3.2.6.1 shows a simplified FT-IR working mechanism. The functional groups present in the sample are shown in the region of wavenumbers over 1500 cm^{-1}, however the plot remains unchanged regardless of whether the *y*-axis on the plot is represented as absorbance or transmittance. This process is useful for identifying a synthesised material, chemical composition and contaminants present in a sample [19, 20].

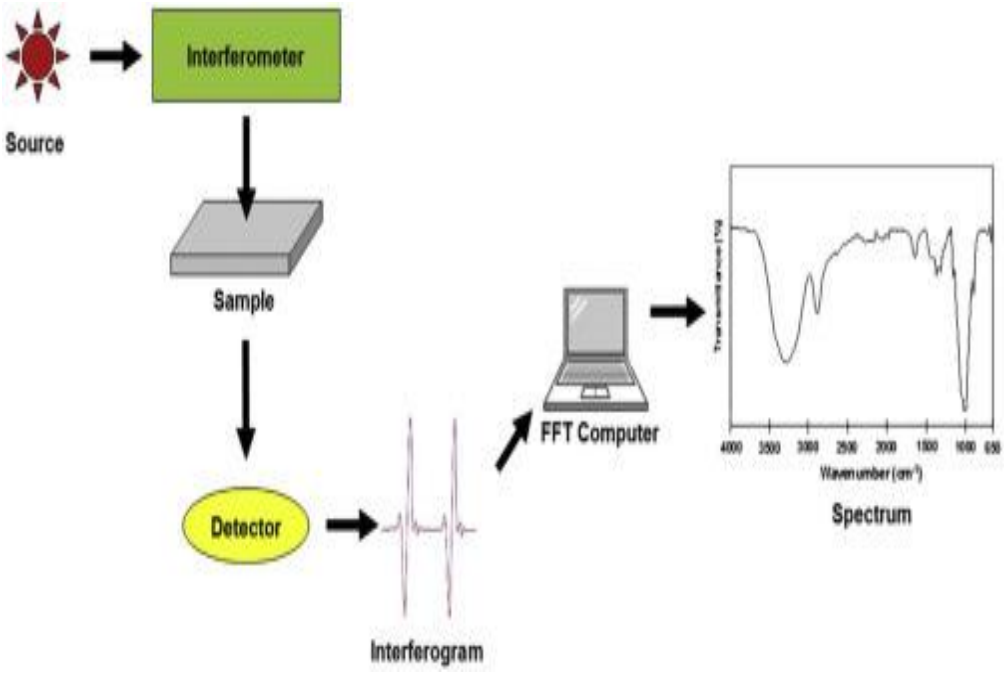

Figure 3.2.6.1: Schematic of FT-IR procedure [19].

Figure 3.2.6.2: The Bruker-ALPHA FT-IR spectrometer.

A certain amount of each V_2O_5 sample of was placed on the sample holder of the Bruker-ALPHA FTIR spectrometer on Figure 3.2.6.2 for the measurement. The samples were scanned at 15-sec measurement time with a resolution of 10 cm^{-1}. The background scan was 24 scans. The interferograms of each V_2O_5 sample had 6012 points in the range of 4000 to 400 cm^{-1} wavenumbers.

3.3. References

[1] L. Nichols, Organic chemistry lab techniques, California: chemistry faculty at Butte Community College in Northern California, 2017.

[2] H. Wang, D. Chen, Y. Cai, R. Zhang, J. Xu, Z. Deng, X. Zheng, Y. Li, I. Bello and B. Su, “Facile synthesis of hierarchical and porous V2O5 microspheres as cathode materials for lithium ion batteries,” *Journal of Colloid and Interface Science,* vol. 418, pp. 74-80, 2014.

[3] S. K. Aditha, A. D. Kurdekar, L. A. Avinash Chunduri, S. Patnaik and V. Kamisetti, “Aqueous based reflux method for green synthesis of nanostructures: Application in CZTS synthesis,” *MethodsX,* vol. 3, pp. 35-42, 2016.

[4] P. P. Pednekar, S. C. Godiyal, K. R. Jadhav and V. J. Kadam, “Mesoporous silica nanoparticles: a promising multifunctional drug delivery system,” in *Nanostructures for Cancer Therapy*, 2017, pp. 593-621.

[5] D. D. Le Pevelen, “Small Molecule X-Ray Crystallography, Theory and Workflow,” *Encyclopedia of Spectroscopy and Spectrometry (Second Edition),* pp. 2559-2576, 2010.

[6] M. F. Manamela, T. E. Mosuang and B. W. Mwakikunga, “Structural, optical and sensing properties of cobalt and indium doped zinc oxide prepared mechano-chemically,” University of Limpopo, Polokwane, 2018.

[7] K. D. Vernon-Parry, “Scanning electron microscopy: an introduction,” *III-Vs Review,* vol. 13, no. 4, pp. 40-44, 2000.

[8] P. E. Stutzman and J. R. Clifton, “Specimen Preparation for Scanning Electron Microscopy,” in *International Conference on Cement and Microscopy*, Las Vegas, 1999.

[9] S. Myat, T. Htay, S. N. Khine, K. S. Oo, T. H. Yin, T. T. Mya and K. P. Tun, “XRD and SEM Analysis, and Semiconductor Type Determination of TiO2 for Dye-sensitized Solar Cell,” *International Research Journal of Advanced Engineering and Science,* vol. 4, no. 2, pp. 103-107, 2019.

[10] C. O. Colpan, Y. Nalbant and M. Ercelik, “Fundamentals of Fuel Cell Technologies,” *Comprehensive Energy Systems,* vol. 4, pp. 1107-1130, 2018.

[11] A. A. Akande, E. C. Linganiso, B. P. Dhonge, K. E. Rammutla, A. Machatine, L. Prinsloo, H. Kunert and B. W. Mwakikunga, “Phase evolution of vanadium oxides obtained through temperature programmed calcinations of ammonium vanadate in hydrogen atmosphere and their humidity sensing properties,” *Materials Chemistry and Physics,* vol. 151, pp. 206-214, 2015.

[12] H. Du, Z. Han, Q. Wang, Y. Gao, C. Gao, J. Dong and X. Pan, “Effects of ferric and manganese precursors on catalytic activity of Fe-Mn/TiO2 catalysts for selective reduction of NO with ammonia at low temperature,” *Environmental Science and Pollution Research,* vol. 27, p. 40870–40881, 2020.

[13] P. Majumdar and S. Patra, “Development of Electrodes for Artificial Photosynthetic System,” Indian Institute of Engineering Science and Technology, Hāora, 2017.

[14] V. Amendola and M. Meneghetti, “Size Evaluation of Gold Nanoparticles by UV-vis Spectroscopy,” *Journal of Physical chemistry,* vol. 113, p. 4277–4285, 2009.

[15] Y. Guo, C. Liu, R. Ye and Q. Duan, “Advances on Water Quality Detection by UV-Vis Spectroscopy,” *Applied Sciences,* vol. 10, no. 19, p. 6874, 2020.

[16] E. K. Grasse, M. H. Torcasio and A. W. Smith, “Teaching UV−Vis Spectroscopy with a 3D-Printable Smartphone Spectrophotometer,” *Journal of Chemical Education,* vol. 93, p. 146−151, 2016.

[17] M. S. Braga, O. Gomes, R. F. Jaimes and E. Braga, “Multispectral colorimetric portable system for detecting metal ions in liquid media,” in *2019 4th International Symposium on Instrumentation Systems, Circuits and Transducers (INSCIT)*, 2019.

[18] S. Vogt , K. Löffler, A. Dinkelacker, B. Bader, I. B. Autenrieth, S. Peter and J. Liese, “Fourier-Transform Infrared (FTIR) Spectroscopy for Typing of Clinical Enterobacter cloacae Complex Isolates,” *Frontiers in Microbiology,* vol. 10, pp. 1-11, 2019.

[19] V. K. Undavalli, C. Ling and B. Khandelwal, “Impact of alternative fuels and properties on elastomer compatibility,” in *Aviation Fuels*, Tuscaloosa, University of Alabama, 2021, pp. 113-132.

[20] V. Chevali and E. Kandare, “Rigid biofoam composites as eco-efficient construction materials,” *Biopolymers and Biotech Admixtures for Eco-Efficient Construction Materials,* pp. 275-304, 2016.

Chapter 4: Results and Discussion

Structural and Optical Properties

4.1. Introduction

V_2O_5 is a significant n-type transition metal oxide semiconductor. With a band gap of 2.2-2.7 eV in the visible region making it a promising candidate for photodetection [1]. Its layered crystal structure, excellent electrical properties, thermal stability, and ease of synthesis make V_2O_5 a promising candidate for a variety of applications [2]. Various morphologies of V_2O_5 such as nanobelts, nanorods, nanosheets, nanoflowers, nanotubes, nanowires and more have been identified as responsible for enhancing the applicability of the material [3]. Employing facile synthesis methods such as sol gel, hydrothermal and spray pyrolysis exhibits the ease of synthesis of V_2O_5 nanostructures which are amorphous when deposited at temperatures lower than 300^oC. Crystallisation, however, depends on the calcination temperature. Akl et. al. [4] reported the deposition of polycrystalline V_2O_5 thin films with orthorhombic crystal structure at 350^oC using spray pyrolysis for optical applications. The V_2O_5 thin films were found to increase in crystallinity with increased annealing temperature. Studies demonstrated that the addition of V_2O_5 in increasing concentrations (0 – 3 wt%) drastically enhances the detection capabilities of V_2O_5-WO_3-TiO_2 (VWT) towards NH_3 for potentiometric detectors [5]. Hydrothermal method remains the simplest and commonly used synthesis technique for V_2O_5 nanostructures in gas detection applications. Having produced various morphologies such as nanoflakes [6], ultrathin nanobelts [7] and more. This current work aims to investigate the structural, optical and gas sensing properties of pure V_2O_5 and Au-doped V_2O_5 using a facile reflux method.

4.2. Structural Characterisation

4.2.1. XRD Results

The phase purity and crystallinity of as-calcined V_2O_5 and Au-doped V_2O_5 at different concentrations from 1 wt% to 5 wt% were examined using the XRD technique. Figure 4.2.1.1 depicts the x-ray diffractograms of all the prepared samples. Figure 4.2.1.1 exhibits sharper peaks as the concentration of Au is increased. This means that the samples become more crystalline as Au concentration increases since all samples were calcined at 300ºC. Similar results have been reported by Najim et al. [8] and Garai et al. [9] There are several diffraction peaks at 2θ angle positions of 15.41º, 20.25º, 26.02º, 31.09º, 41.75º corresponding precisely to planes (200), (001), (110), (400) and (020) respectively. This confirms that the V_2O_5 samples possess a Shcherbianaite orthorhombic crystal structure in the P_{mmn}(59) space group - according to the Crystallographic Open Database (COD) entry number 96-901-2222 [10].

There are no peaks corresponding to Au that were observed in the x-ray diffractograms of the 1 wt% to 4 wt% Au-doped V_2O_5 samples to indicate that the Au ions have substituted the V_2O_5 ions at low Au concentrations in the V_2O_5 nanoparticles. Sustainably similar findings were reported by Liang et al. [11] and Maswanganye et al. [12], however, the peak at 38.19º for 5 wt% Au-doped V_2O_5 diffractogram is speculated to correspond to (111) plane of Au due to interstitial doping during synthesis according to the COD entry number 96-901-3045 [13]. The 2 wt% Au-doped V_2O_5 sample shows an intense peak at 10.58 º which is an impurity peak from mercury. Similar results were reported by [14]

Debye Scherrer's equation and the equation relating the d-spacing with miller indices (hkl) for orthorhombic crystal materials were used, to estimate the crystallite sizes and the lattice parameters respectively. The values were recorded in Table 2 and the lattice

parameters of Au-doped V_2O_5 diverge from the values of undoped V_2O_5 by a small to negligible amount. The crystallite size of V_2O_5 increase from 14.25nm to 20.80nm at low Au concentrations of 1 wt% to 3 wt% and tend to decrease from 20.80nm to 8.32nm at higher Au concentrations of 4 wt% to 5 wt%. This may be due to the increased number of nucleation sites present at high Au concentrations resulting in a reduced crystallite size compared to lower Au concentrations during refluxing [15]. The findings demonstrate the reflux method's applicability for doping of V_2O_5 nanostructures.

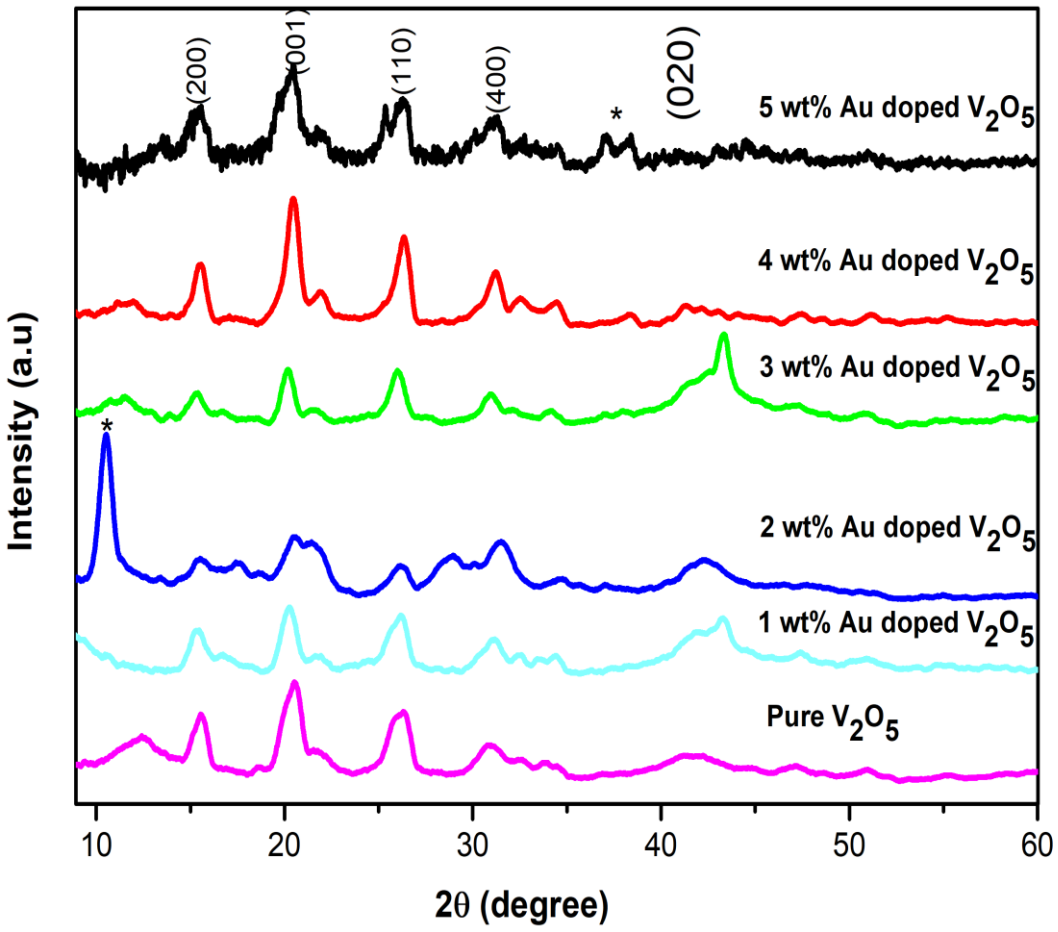

Figure 4.2.1.1: The XRD plots for all refluxed samples

Table 2: *Determined crystallite sizes and lattice parameters*

Name of sample	Crystallite size (nm)	Lattice parameters (Å)		
		a	b	c
Pure V_2O_5	14.25	11.48	3.57	4.34
1% Au doped V_2O_5	16.41	11.49	3.58	4.38
2% Au doped V_2O_5	18.87	11.47	3.61	4.36
3% Au doped V_2O_5	20.80	11.56	3.59	4.40
4% Au doped V_2O_5	17.19	11.43	3.55	4.34
5% Au doped V_2O_5	8.32	11.55	3.59	4.38

4.2.2. Scanning Electron Microscopy (SEM)

The FEI Quanta 400 FEG-ESEM was used to examine the morphological features of the as-calcined V_2O_5 nanoparticles. Figure 4.2.2.1 shows the morphology of the prepared V_2O_5 and Au-doped V_2O_5 nanoparticles prepared from NH_4VO_3, $HAuCl_4$ solution and ethylene glycol (EG). The purple vanadyl ethylene glycolate (VEG) formed during refluxing under continuous stirring and rinsing with alcohol was calcined at 300^oC and converted to V_2O_5 nanospheres that appear interconnected and assembled by nanorod-like structures as observed in Figure 4.2.2.1 (a-b). The doping of the $HAuCl_4$ solution at various concentrations decomposes the nanospheres to nanorods of non-uniformly distributed lengths ranging from 209-577nm as shown in Figure 4.2.2.1 (c-k). The $HAuCl_4$ solution at low concentrations behaves like an acid as Figure 4.2.2.1 (c-d) shows no signs of nanosphere-like morphology as reported by Borgekov et al. [16], while also confirming the mixture of reagents affects the morphology of a material.

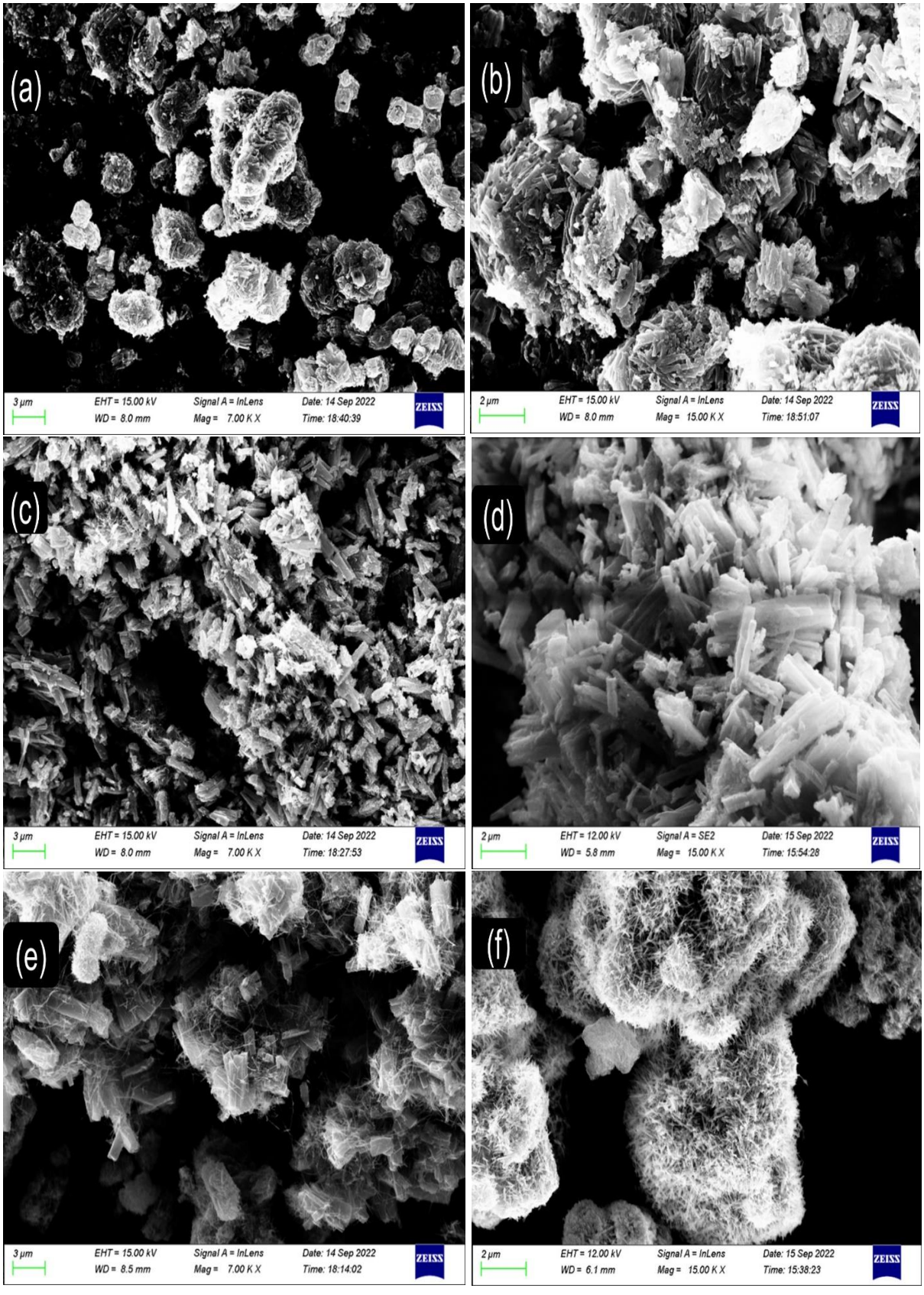
(a)
3 µm EHT = 15.00 kV Signal A = InLens Date: 14 Sep 2022
WD = 8.0 mm Mag = 7.00 K X Time: 18:40:39
ZEISS
(b)
2 µm EHT = 15.00 kV Signal A = InLens Date: 14 Sep 2022
WD = 8.0 mm Mag = 15.00 K X Time: 18:51:07
ZEISS
(c)
3 µm EHT = 15.00 kV Signal A = InLens Date: 14 Sep 2022
WD = 8.0 mm Mag = 7.00 K X Time: 18:27:53
ZEISS
(d)
2 µm EHT = 12.00 kV Signal A = SE2 Date: 15 Sep 2022
WD = 5.8 mm Mag = 15.00 K X Time: 15:54:28
ZEISS
(e)
3 µm EHT = 15.00 kV Signal A = InLens Date: 14 Sep 2022
WD = 8.5 mm Mag = 7.00 K X Time: 18:14:02
ZEISS
(f)
2 µm EHT = 12.00 kV Signal A = InLens Date: 15 Sep 2022
WD = 6.1 mm Mag = 15.00 K X Time: 15:38:23
ZEISS

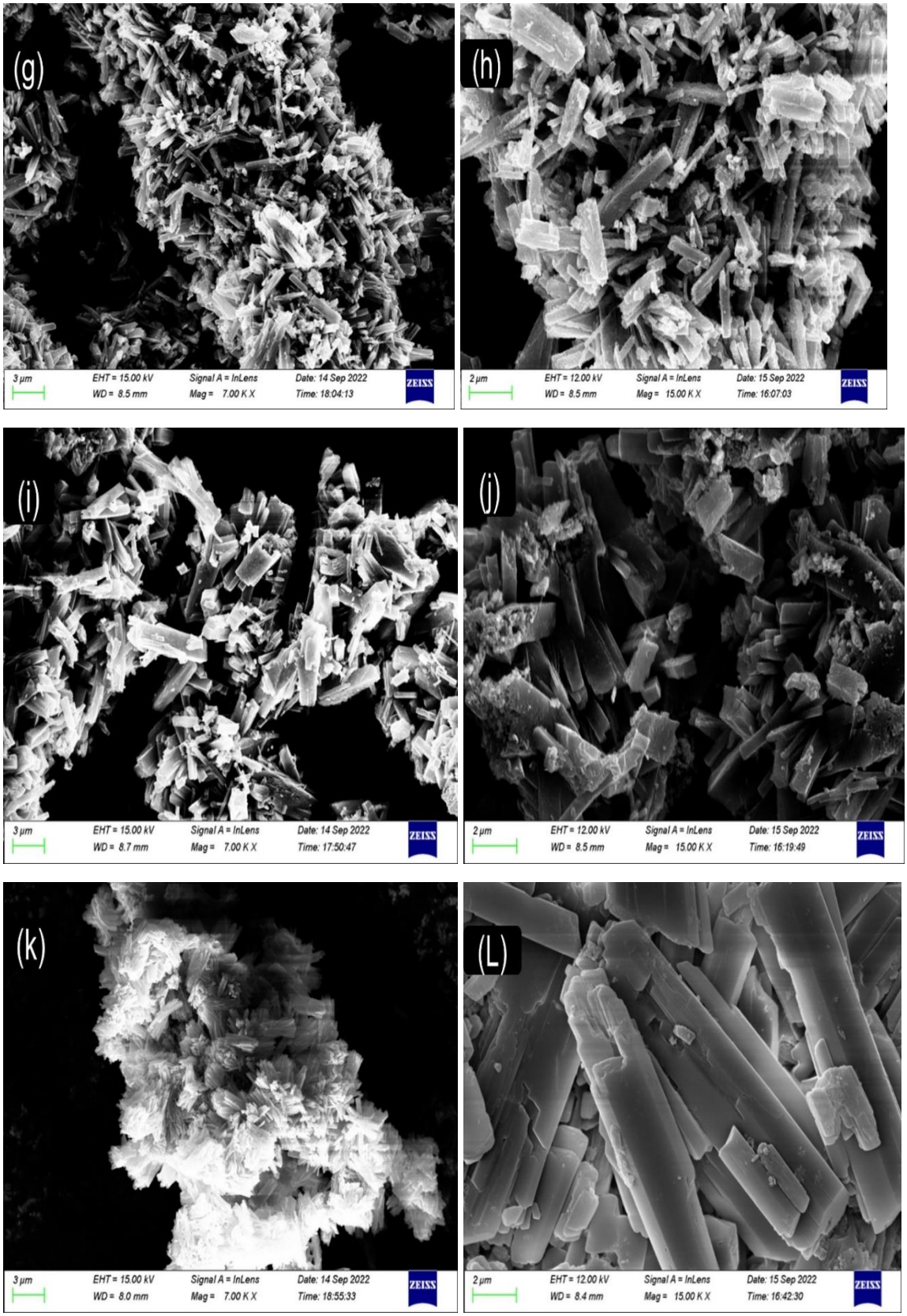

Figure 4.2.2.1: (a-b) SEM images of undoped V_2O_5 sample (c-d) SEM images of 1 wt% Au-doped V_2O_5 sample (e-f) SEM images of 2 wt% Au-doped V_2O_5 sample (g-h) SEM images of 3 wt% Au-doped V_2O_5 sample (i-j) SEM images of 4 wt% Au-doped V_2O_5 sample (k-l) SEM images of 5 wt% Au-doped V_2O_5 sample.

The 2% Au doped V_2O_5 shows the nanorods covered in nanowire-like structures with diameters between 42nm – 52nm in Figure 4.2.2.1(e-f) due to contamination of mercury (Hg) resulting in a high surface area also confirmed by the EDS. The presence of the silver metallic element Hg is attributed to this phenomenon and similar findings were reported by Solis-Casados et al. [17]. The Au-doped V_2O_5 nanorod-like nanostructures having a rough surface grow bigger as the Au concentration is increased. These findings are consistent with those of Pan et al. [18], who claimed that altering the volume of ethylene glycol has an impact on the surface texture (roughness/smoothness) of the nanostructures. Figure 4.2.2.1 shows that the surface texture of the V_2O_5 nanostructures are unaffected by variations in the concentration of Au since the volume of ethylene was kept at 50mL for all samples. The agglomeration of the V_2O_5 nanorods occurs at higher concentration of Au (4 wt% to 5 wt%) and a reduced surface area as shown in Figure 4.2.2.1 (i-L) can be attributed to the high surface binding energy of Au as stated in literature since no capping reagents were used in this work [19]. Agglomeration tends to distort the hollow nature of the V_2O_5 nanostructures at high Au concentrations which may limit the applicability of the material in various applications.

4.2.3. Energy Dispersive X-Ray Spectroscopy (EDS)

The elemental composition of the prepared nanostructures was confirmed using the energy dispersive spectroscopy (EDS). Figure 4.2.3.1 (a-f) and Table 3 shows each element and the respective weight percentage constituted in each of the six prepared V_2O_5 samples. All the prepared samples show the existence vanadium (V) with several peaks and oxygen (O) as V_2O_5 is the parent material. The minority peak within 0 – 1 keV is due to carbon (C) which was used to coat the samples. Figure 4.2.3.1 (c) shows the presence of Hg in the material due to contamination on the 2 wt% Au-doped V_2O_5

samples. The existence of Au is observed at higher concentrations of 4 wt% and 5 wt%, However, at lower Au concentrations (1 wt% - 3 wt%) the Au element was not observed. This indicates that the Au nanoparticles grow at higher concentrations of $HAuCl_4$ solution when using the reflux method.

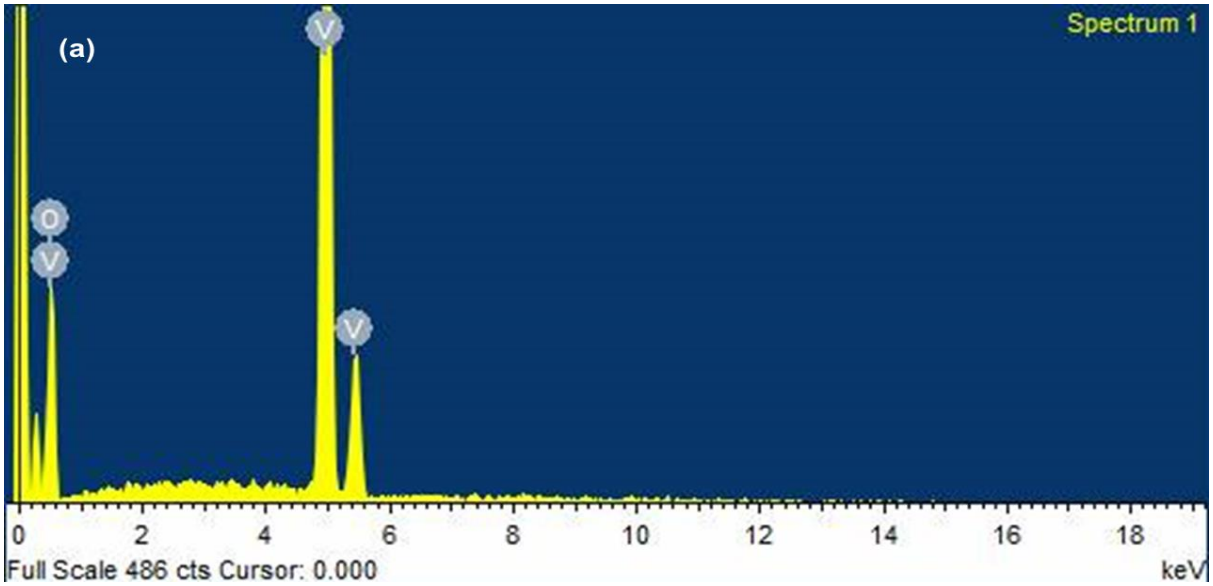

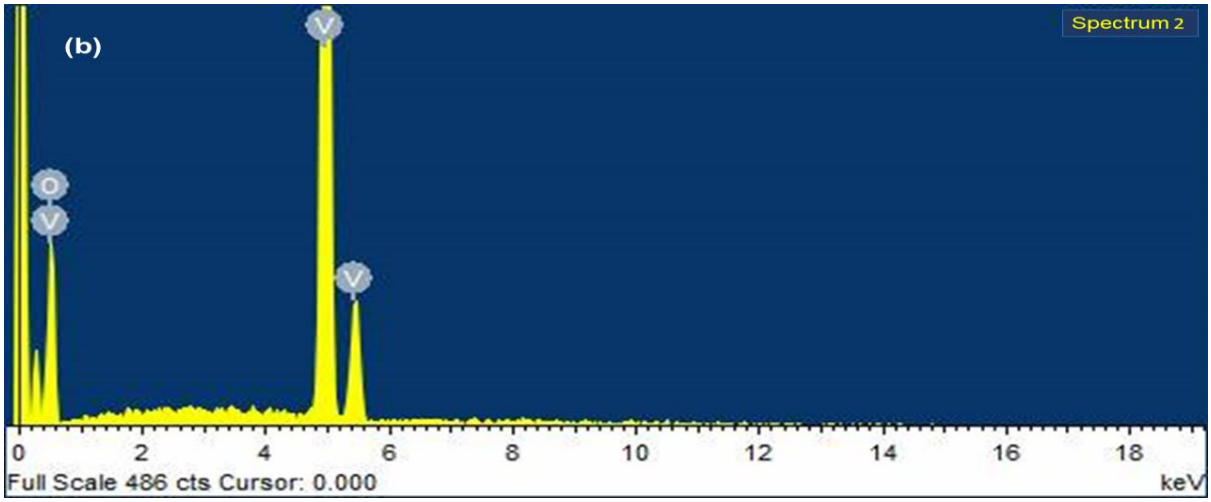

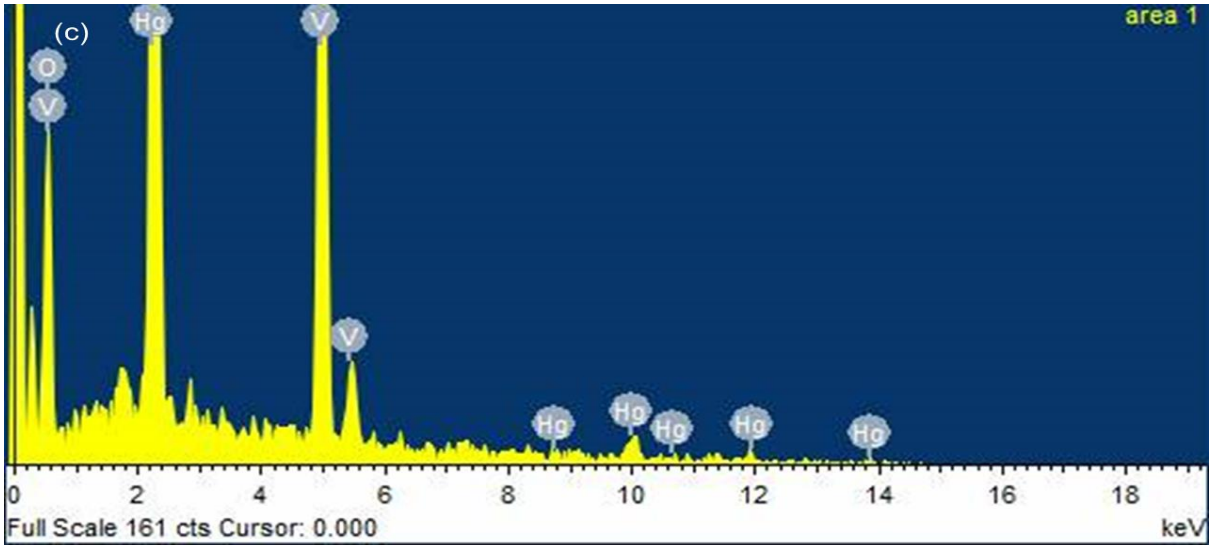
(c)
area 1
O
V
Hg
V
V
Hg
Hg
Hg
Hg
Hg
0 2 4 6 8 10 12 14 16 18
Full Scale 161 cts Cursor: 0.000
keV

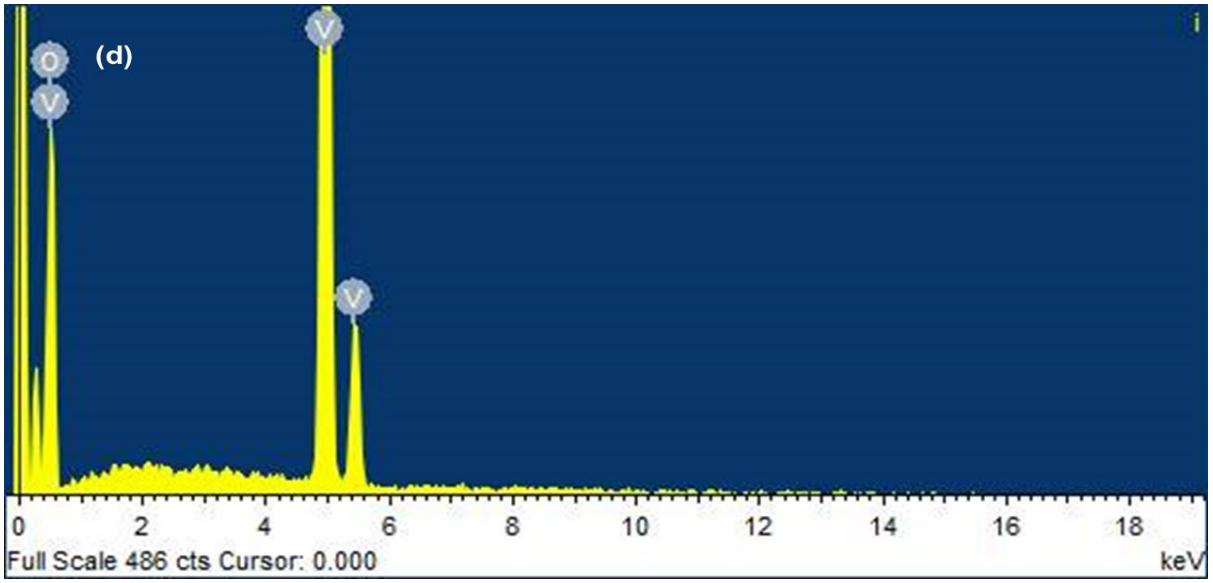
(d)
i
O
V
V
V
0 2 4 6 8 10 12 14 16 18
Full Scale 486 cts Cursor: 0.000
keV

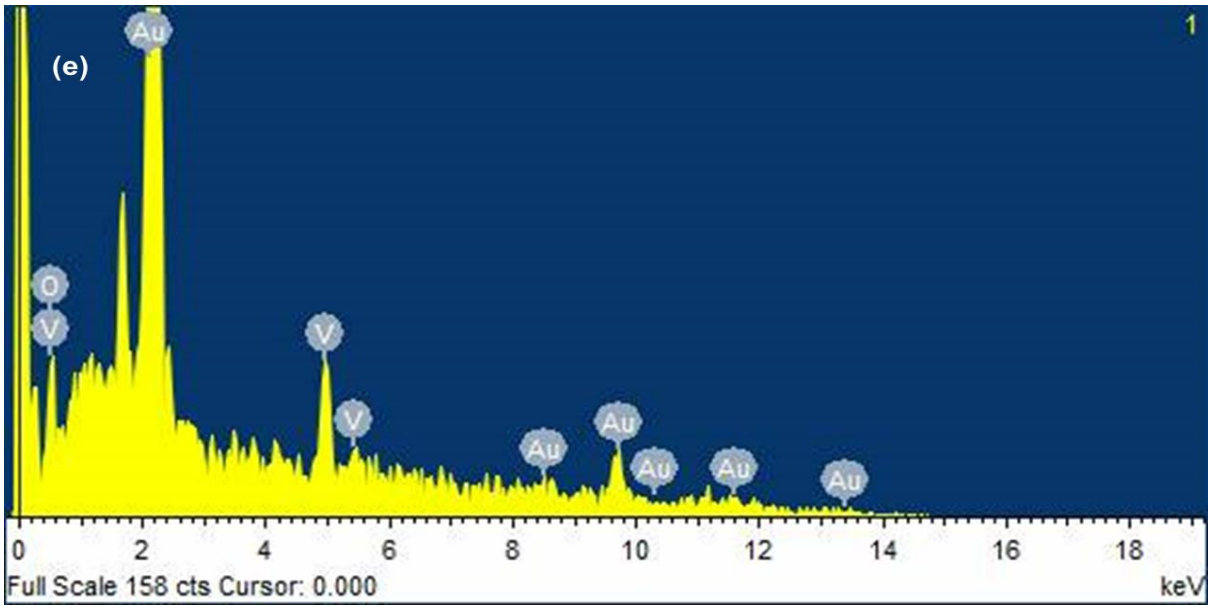
(e)
1
Au
O
V
V
V
Au
Au
Au
Au
Au
0 2 4 6 8 10 12 14 16 18
Full Scale 158 cts Cursor: 0.000
keV

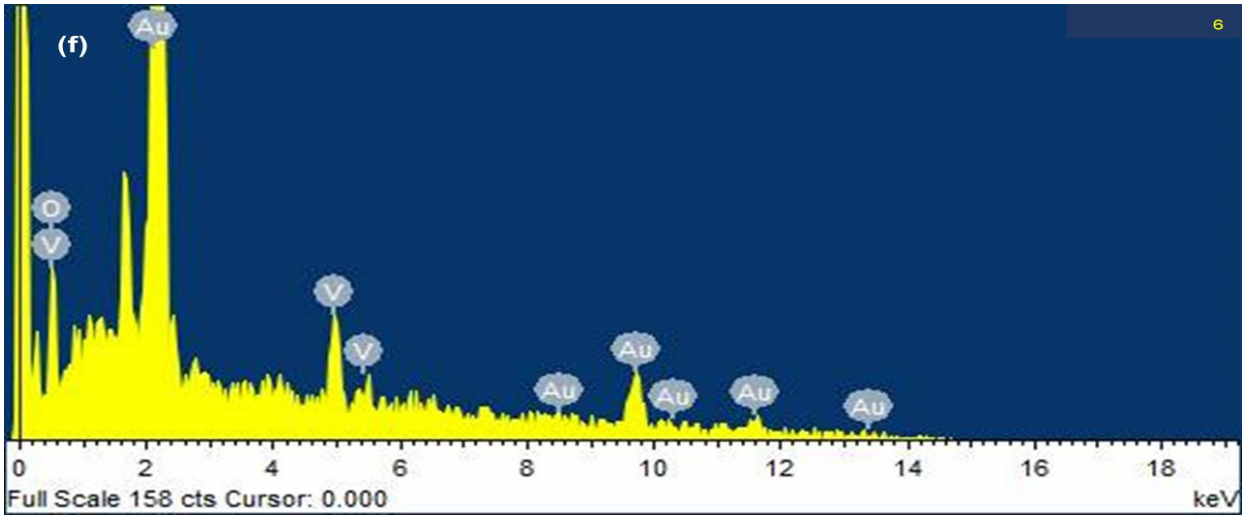

Figure 4.2.3.1: The EDS spectrum of all V_2O_5 samples

Table 3: Elemental composition in percentages for all prepared samples

Sample name		Elemental content (%)			
	V	O	C	Au	Hg
Pure V_2O_5	60.35	31.63	8.02	-	-
1 wt% Au-doped V_2O_5	59.38	29.32	11.30	0.00	-
2 wt% Au-doped V_2O_5	50.34	11.80	10.00	0.00	27.86
3 wt% Au-doped V_2O_5	54.70	38.08	7.22	0.00	-
4 wt% Au-doped V_2O_5	57.47	25.35	9.20	7.98	-
5 wt% Au-doped V_2O_5	45.67	26.33	12.05	15.95	-

4.2.4. Brunuaer-Emmett-Teller (BET) Surface Area Analysis

Prior to BET experiment in the Tristar II instrument, the samples were degassed at 120^{o}C for 2 hours to remove moisture or contaminants. Liquid N_2 was introduced as an adsorbent at 77K to determine the specific surface area, pore volume and pore size. Figure 4.2.4.1 reveals that all samples exhibit Type II isotherm characteristics within the relative pressure (P/P_o) ranging from 0.0 to around 0.75, however the

samples exhibit Type IV isotherm characteristics at (P/P_o) ≥ 0.75 and H3 type hysteresis. These suggest that all samples are mesoporous materials and have slit-like pores made of non-rigid platelet aggregates according to IUPAC classification. Figure 4.2.4.2 shows the pore size distribution against differential volume (dv/dlog (D)). The determined values for pore volume, pore size and specific surface area are listed in Table 4 for all the samples. The surface area of the V_2O_5 samples tend to increase at low concentrations of Au (1 wt% – 2 wt%) and decrease as the concentration of Au increases (3 wt% – 5 wt%). The straight-line plot of the V_2O_5 sample doped with 2 wt% Au in figure 4.2.4.3 has a low intercept value and slope of the plot, which is vice versa for 5 wt% Au doped sample since it has the lowest surface area among the samples.

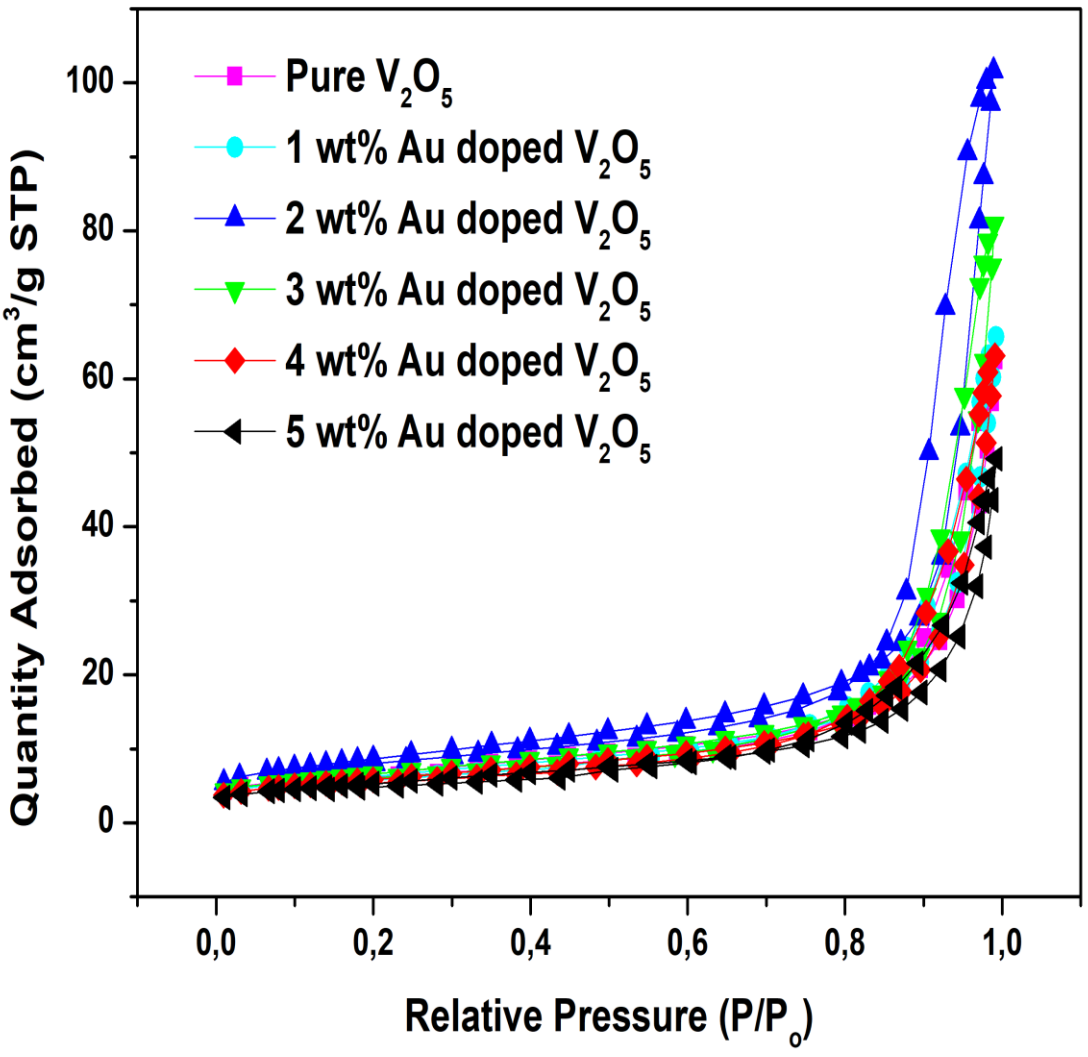

Figure 4.2.4.1: N_2 adsorption and desorption isotherm of all prepared samples.

Table 4: *Values of BET surface area and average pore size.*

Sample Name	Slope (g/cm^3 STP)	Intercepts (g/cm^3 STP)	BET constant (c)	Pore diameter (nm)	Specific Surface Area(m^2/g)	Pore Volume (cm^3/g)
Pure V_2O_5	0.19	0.000970	191.85	8.70	23.03	0.09
1 wt% Au doped V_2O_5	0.19	0.001263	153.98	9.59	22.39	0.10
2 wt% Au doped V_2O_5	0.14	0.000894	158.82	11.53	30.67	0.16
3 wt% Au doped V_2O_5	0.18	0.001455	126.75	10.53	23.61	0.12
4 wt% Au doped V_2O_5	0.21	0.001483	140.70	10.18	20.86	0.10
5 wt% Au doped V_2O_5	0.23	0.001504	153.99	8.65	18.80	0.08

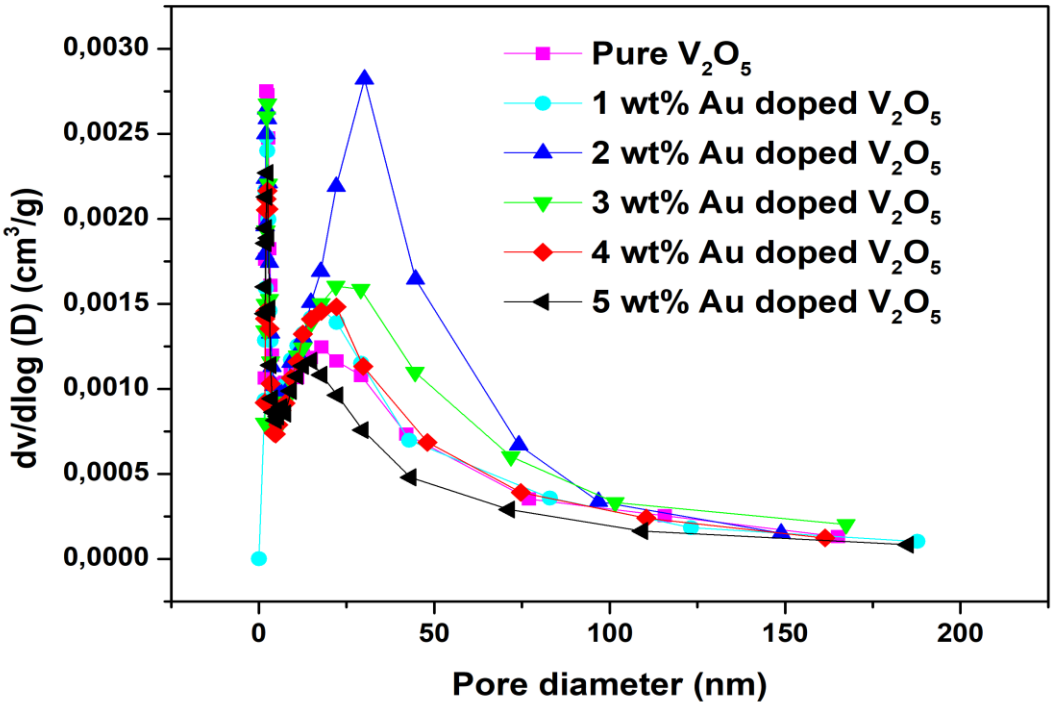

Figure 4.2.4.2: BJH pore size distribution of all samples.

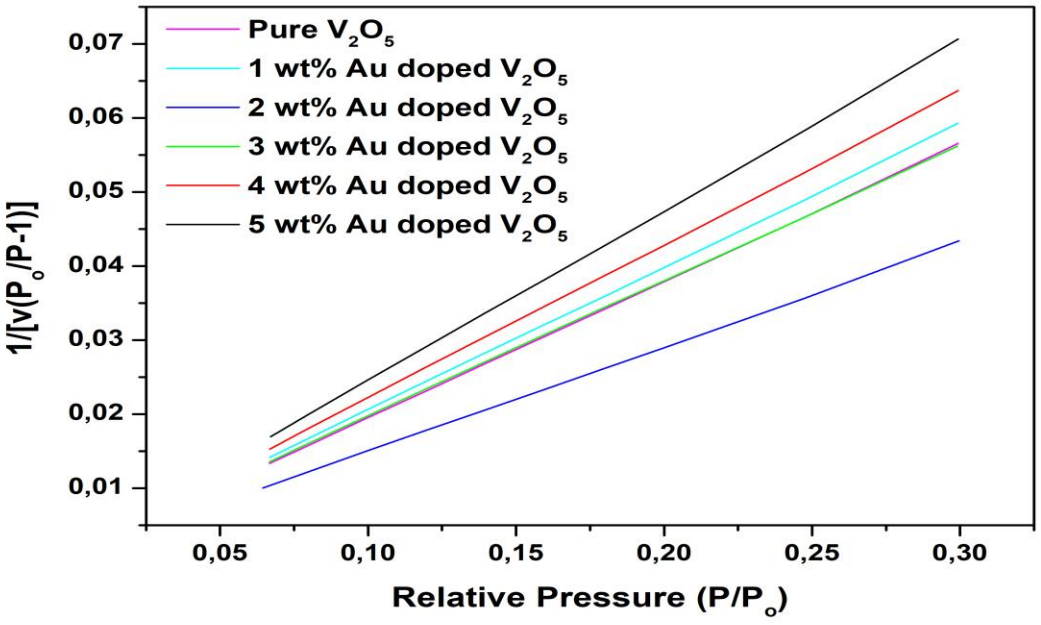

Figure 4.2.4.3: Surface area straight line plots for all V_2O_5 samples.

4.3. Optical Characterisation

4.3.1. Ultraviolet-Visible Spectroscopy

The optical behaviour of the V_2O_5 samples in the ultraviolet and visible light region was investigated using Perkin Elmer UV-Vis spectrophotometer SP-UV 500. The optical band gaps of undoped V_2O_5 and Au doped V_2O_5 samples calcined at 300ºC was determined from the cut-off wavelength obtained from the resultant UV-Vis spectrum and substituting in the Plank's relation equation below [20, 21, 22]:

$$E_g = h\nu_g = \frac{hc}{\lambda} \qquad 2.2.1.1$$

Where *c* is the speed of light, (3×10^8 m.s^{-1}), *h* is the Max Planck's constant (6.63 x 10^{-34} J.s), *λ* is the cut-off wavelength in nanometers (nm) of each sample and E_g is the band gap of the material. The cut-off wavelength corresponding to each sample's UV-Vis spectra at the point of intersection with the x-axis is indicated by the straight lines extending diagonally from each sample's spectrum. The determined band gaps were found to be within the range of 3.10 – 3.53 eV and tabulated in Table 5 along with the cut-off wavelengths within the range of 351.71 - 400.00 nm. Deepak Raj et al. [23] reported DC magnetron sputtered V_2O_5 thin films with wide optical band gaps in the range 2.5 to 3.49 eV. Singh et al. [24] reported the sol gel synthesised pure and Sn doped V_2O_5 nanoparticles with wide optical band gaps within the range of 3.27 eV to 3.07 eV. Due to the Moss-Burstein effect, which causes the band gap to widen, the optical band gap dependency on the amount of dopant Au in V_2O_5 can be attributed [24]. The calculated band gaps were found to be greater than the normally reported band gap for bulk V_2O_5 2.38 eV with a cut-off wavelength of 522nm [25]. V_2O_5 requires to absorb photons with energies equivalent to or higher than the band gap energy in order to form active photocatalytic entities. Compared to pure V_2O_5 and V_2O_5 doped

at 1 wt%, 3 wt%, 4 wt%, and 5 wt% Au, the 2 wt% Au-doped V_2O_5 has the smallest band gap of 3.10 eV. Bulk V_2O_5 was found to possess a narrower band gap when compared undoped and Au-doped V_2O_5 in this work. The optical behaviour of the samples as shown in Figure 4.3.1.1 reveals a negligible decrease in absorbance at lower concentrations of Au and a huge drop in absorbance at higher concentrations of Au recorded in the wavelength range of 200nm – 400nm at room temperature. Similar results of a decrease in transmittance with an increase in precursor concentration for V_2O_5 thin films by Gavalas et al. [26]. The 2 wt% Au-doped V_2O_5 sample exhibited the highest absorbance compared to all the experimental samples due to the presence of Hg affecting the optical behaviour. The co-doping effect of Au and Hg is suspected to improve the photo absorption of the 2 wt% sample. This sample has a band gap of 3.1 eV with a cut-off wavelength of 400nm suggesting it can be applicable for photocatalysis [27].

Table 5: *Sample dopant concentration, energy gap and cut-off wavelength for all samples*

Sample name	Concentration (by wt %)	Cut-off wavelength (nm)	Energy band gap (eV)
V_2O_5	0	385.41	3.22
1 wt% Au doped V_2O_5	1	387.65	3.20
2 wt% Au doped V_2O_5	2	400.00	3.10
3 wt% Au doped V_2O_5	3	385.41	3.22
4 wt% Au doped V_2O_5	4	376.41	3.29
5 wt% Au doped V_2O_5	5	351.71	3.53
Bulk V_2O_5	-	522.00	2.38 [25]

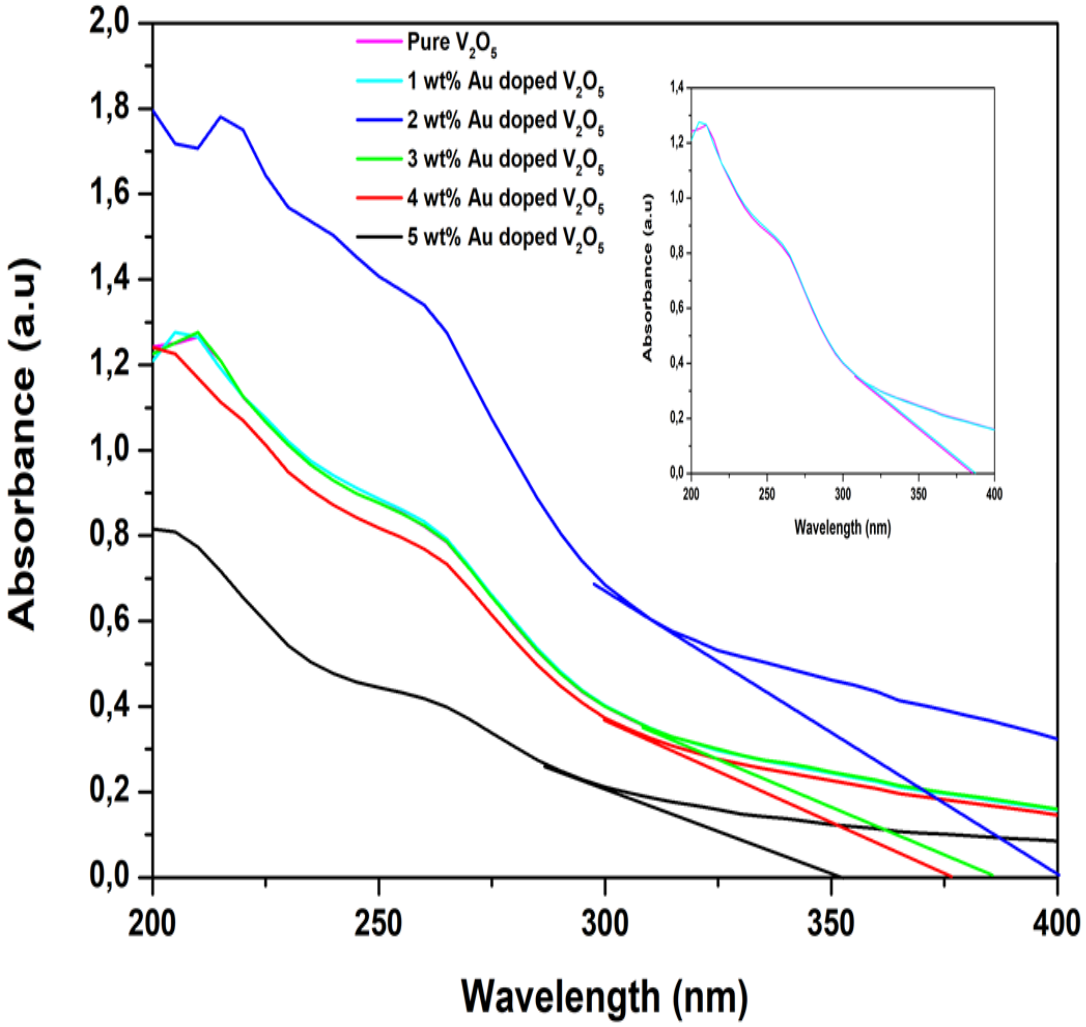

Figure 4.3.1.1: The optical absorption spectra of undoped V_2O_5 and Au-doped V_2O_5 samples. The inset figure shows the spectra for undoped and 1wt% Au-doped V_2O_5.

4.3.2. Fourier Transform Infrared spectroscopy (FT-IR)

The functional groups present in the prepared V_2O_5 samples were examined using FT-IR spectroscopy .Figure 4.3.2.1 shows the FT-IR spectra for all refluxed V_2O_5 samples with significant bands at wavenumbers 417.12 cm^{-1}, 576.16 cm^{-1}, 796.20 cm^{-1} and 986.81 cm^{-1} corresponding to the V-O coordination chemistry of single crystalline V_2O_5 nanostructures. The oxygen stretching modes, which are shared by three vanadium atoms, have been attributed to the band that occurred at 417.12 cm^{-1}

according to Jadhav et al. [28]. The bands at wavenumbers 576.16 cm^{-1} and 796.20 cm^{-1} are due to the bridging oxygen atom bonded to two vanadium atoms with stretching mode V-O-V according to Kumar et al. [29]. The symmetric V=O mode of V_2O_5, which corresponds to the terminal oxygen tightly bound to just one vanadium atom, is attributed by the band at 986.81 cm^{-1} [30]. Due to the intercalation of Au into the atomic structure of V_2O_5 and the resulting deformation of V-O bonds, the intensity of the peaks decreases as Au concentration is increased and the peaks are slightly shifted to the right-hand side of the spectrum from 986.81 cm^{-1} to 1019.83 cm^{-1}. The spectrum for the 2% Au-doped sample clearly differs from the other samples due to the presence of mercury (Hg) resulting in a doublet band at around 1000 cm^{-1} material of V_2O_5. The peak at 652.48 cm^{-1} is indicative of the Hg-O bond stretching [31, 32].

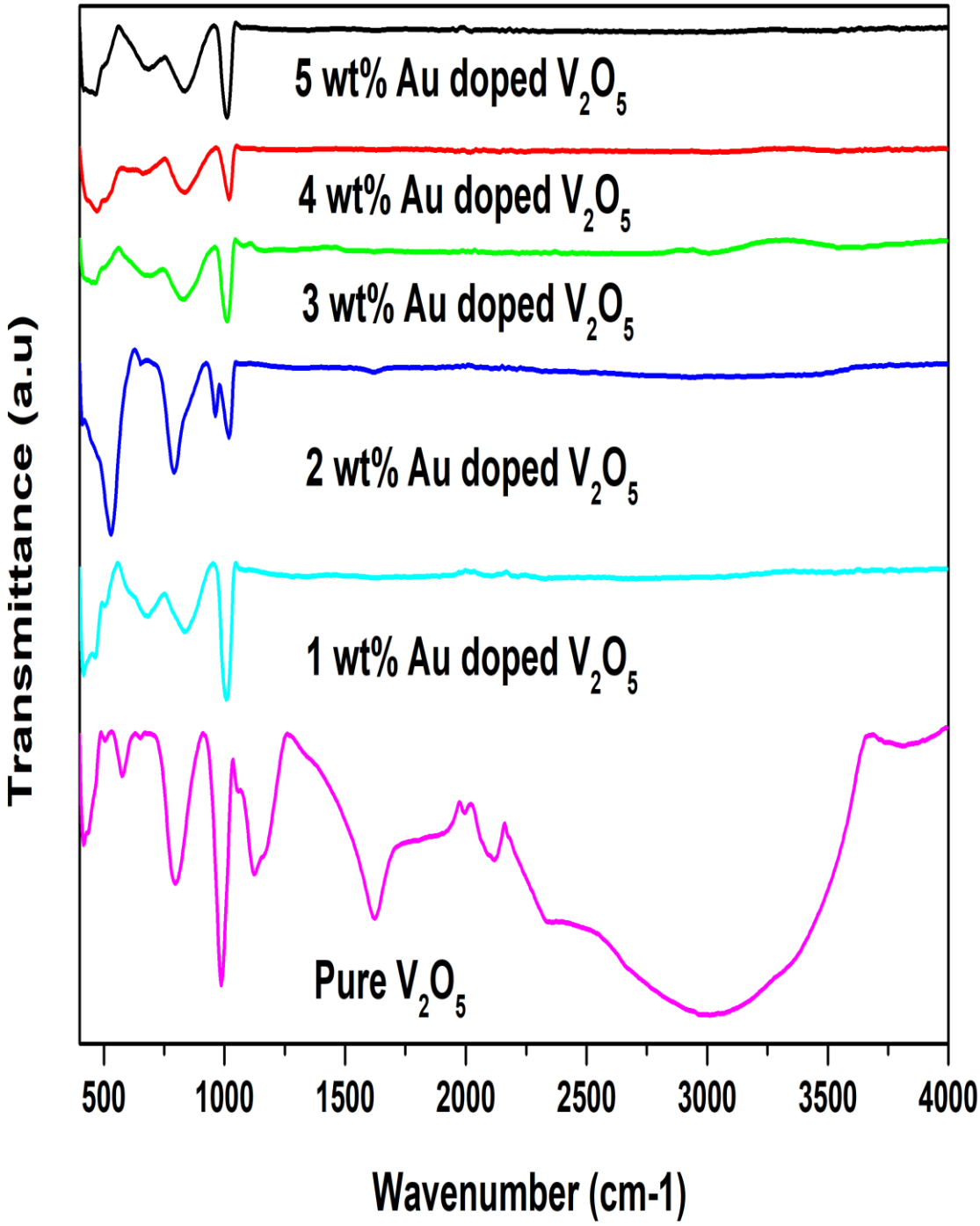

Figure 4.3.2.1: FT-IR spectra of undoped V_2O_5 and Au-doped V_2O_5 at concentrations ranging from 1 wt% to 5 wt%.

4.5 References

[1] M. Al Zoubi, H. K. Farag and F. Endres, "Sol-gel synthesis of vanadium pentoxide nanoparticles in air- and water-soluble ionic liquids," *Journal of Materials Science,* vol. 44, no. 5, pp. 1363-1373, 2009.

[2] N. M. Abd-Alghafour, N. M. Ahmed and Z. Hassan, "Fabrication and characterization of V2O5nanorods based metal–semiconductor–metal photodetector," *Sensors and Actuators A: Physical,* vol. 250, pp. 250-257, 2016.

[3] V. Mounasamy, G. Kumar Mani and S. Madanagurusamy, "Vanadium oxide nanostructures for chemiresistive gas and vapour sensing: a review on state of the art," *Microchimica Acta,* vol. 187, p. 253, 2020.

[4] A. A. Akl, "Thermal annealing effect on the crystallization and optical dispersion of sprayed V2O5 thin films," *Journal of Physics and Chemistry of Solids,* vol. 71, p. 223–229, 2010.

[5] D. Schonauer-Kamin, M. Fleischer and R. Moos, "Influence of V2O5 content of the catalyst layer of a non-nernstian NH3 sensor," *Solid State Ionics,* pp. 270-273, 2014.

[6] M. S. Mamabolo, Z. P. Tshabalala, H. C. Swart, G. E. Mphaphuli, T. K. Hillie and D. E. Motaung, "Low Temperature Tunability on CO Selectivity, Low Detection Limit Based on SnO2-Hollowspheres Induced by Various Bases," *Surfaces and Interfaces,* vol. 31, p. 101954, 2022.

[7] Y. Qin, L. Zhao and M. Cui, "Ultrathin vanadium pentoxide nanobelt for ethanol-sensing applications: Experimental and ab initio study," *Journal of Alloys and Compounds,* vol. 735, pp. 1480-1487, 2018.

[8] S. A. Najim, N. Y. Jamil and K. M. Muhammed, "Effect of Au Dopant on the Structural and Optical Properties of ZnO Thin Films Prepared by CVD," *Journal of nano- and electronic physics,* vol. 11, no. 2, p. 02003, 2019.

[9] M. Garai, T. S. Murthy and B. Karmakar, "Microstructural Characterization and Wear Properties of Silver and Gold Nanoparticle Doped K-Mg-Al-Si-O-F Glass-ceramics," *Ceramics international,* 2018.

[10] J. A. Ketelaar, "Die Kristallstruktur des Vanadiumpentoxyd," *Zeitschrift fuer Kristallographie,* vol. 95, pp. 9-27, 1936.

[11] J. Liang, J. Liu, N. Li and W. Li, "Magnetron sputtered Au-decorated vanadium oxides composite thin films for methane-sensing properties at room temperature," *Journal of Alloys and Compounds,* vol. 671, pp. 283-290, 2016.

[12] M. W. Maswanganye, T. E. Mosuang, K. E. Rammutla and B. W. Mwakikunga, "The effect of Co (cobalt) and In (indium) combinational doping on the structural and optical properties of ZnO nanoparticles," University of Limpopo, Polokwane, 2017.

[13] I. Suh, H. Ohta and Y. Waseda, "High-temperature thermal expansion of six metallic elements measured by dilatation method and X-ray diffraction," *Journal of material science,* vol. 23, pp. 757-760, 1988.

[14] P. Rompalski, A. Smoliński, H. Krztoń, J. Gazdowicz, N. Howaniec and L. Róg, "Determination of mercury content in hard coal and fly ash using X-ray diffraction and scanning electron microscopy coupled with chemical analysis," *Arabian Journal of Chemistry,* vol. 12, no. 8, pp. 3927-3942, 2019.

[15] F. A. Pineda, N. Budini, R. R. Koropecki and R. D. Arce, "Structural Analysis of ZnO(:Al,Mg) Thin Films by X-ray Diffraction," *Procedia Materials Science,* vol. 8, pp. 551-560, 2015.

[16] D. B. Borgekov, M. V. Zdorovets, A. L. Kozlovskiy, M. D. Kutuzau, E. E. Shumskaya and E. Y. Kaniukov, "Effect of Acidity on the Morphology, Structure, and Composition of Ni Nanotubes," *PHYSICAL CHEMISTRY OF NANOCLUSTERS AND NANOMATERIALS,* vol. 93, no. 1, p. 125–128, 2019.

[17] D. A. Solis-Casados, L. Escobar-Alarcon, A. Infantes-Molina, T. Klimova, L. Serrato-Garcia, E. Rodriguez-Castellon, S. Hernandez-Lopez and A. Dorazco-Gonzalez, "Synthesis and Characterization of Ag-Modified V2O5 Photocatalytic Materials," *Journal of Chemistry,* 2017.

[18] A. Pan, T. Zhu, H. B. Wu and X. W. Lou, "Template-Free Synthesis of Hierarchical Vanadium-Glycolate Hollow Microspheres and Their Conversion to V2O5 with Improved Lithium Storage," *Chemistry A European Journal,* vol. 19, p. 494 – 500, 2013.

[19] O. Długosz, K. Szostak, A. Staroń, J. Pulit-Prociak and M. Banach, "Methods for Reducing the Toxicity of Metal and Metal Oxide NPs as Biomedicine," *Materials (Basel),* vol. 13, no. 2, p. 279, 2020.

[20] D. Sharma, S. Sharma, B. S. Kaith, J. Rajput and M. Kaur, "Synthesis of ZnO nanoparticles using surfactant free in-air and microwave method," *Applied Surface Science,* vol. 257, no. 22, pp. 9661-9672, 2011.

[21] M. F. Manamela, T. E. Mosuang and B. W. Mwakikunga, "Structural, optical and sensing properties of cobalt and indium doped zinc oxide prepared mechano-chemically," University of Limpopo, Polokwane, 2018.

[22] J. Huotari, J. Lappalainen, J. Puustinen and A. Lloyd Spetz, "Gas sensing properties of pulsed laser deposited vanadium oxide thin films with various crystal structures," *Sensors and Actuators B: Chemical,* vol. 187, pp. 386-394, 2013.

[23] P. Deepak Raj, S. Gupta and M. Sridharan, "Influence of the crystalline nature of growing surface on the properties of vanadium pentoxide thin films," *Ceramics International,* 2017.

[24] N. Singh, A. Umar, N. Singh, H. Fouad, O. Y. Alothman and F. Z. Haque, "Highly sensitive ammonia gas sensor based on Sn Doped V2O5 Nanoparticles," *Materials Research Bulletin,* vol. 108, pp. 266-274, 2018.

[25] A. A. Mane and A. V. Moholkar, "Effect of film thickness on NO2gas sensing properties of sprayed orthorhombic nanocrystalline V2O5thin films," *Applied Surface Science,* vol. 416, pp. 511-520, 2017.

[26] S. Gavalas, E. Gagaoudakis, D. Katerinopoulou, V. Petromichelaki, S. Wight, G. Wotring, E. Aperathitis, G. Kiriakidis and V. Binas, "Vanadium oxide nanostructured thin films prepared by Aerosol Spray Pyrolysis for gas sensing

and thermochromic applications," *Materials Science in Semiconductor Processing,* vol. 89, pp. 116-120, 2019.

[27] O. O. Nubi, K. E. Rammutla and T. E. Mosuang, "Single and Double Doping of Nanostructured Titanium Dioxide with Silver and Copper: Structural, Optical and Gas-Sensing Properties," University of Limpopo, Polokwane, 2016.

[28] C. D. Jadhav, B. Pandit, S. S. Karade, B. R. Sankapal and P. G. Chavan, "Enhanced field emission properties of V2O5/MWCNTs nanocomposite," *Applied Physics A,* vol. 124, p. 794, 2018.

[29] A. Kumar and P. P. Sahay, "Influence of Ti doping on the microstructural and electrochromic properties of dip-coated nanocrystalline V2O5 thin films," *Journal of Sol-Gel Science and Technology,* vol. 95, pp. 34-51, 2020.

[30] D. Mei, L. Li, C. Zhu, X. Zhao and Y. Yuan, "Phy-chemical Attributes of Nano-scale V2O5/TiO2 Catalyst and Its' Effect on Soot Oxidation," *Bulletin of Chemical Reaction Engineering & Catalysis,* vol. 11, no. 2, pp. 161-169, 2016.

[31] M. U. Flores, I. A. Reyes, E. G. Palacios, F. Patino, J. C. Juarez, M. Reyes, A. M. Teja, H. Islas and E. J. Gutierrez, "Kinetic Analysis of the Thermal Decomposition of aSynthetic Mercury Jarosite," *Minerals,* vol. 9, no. 200, 2019.

[32] Y. M. de Matos, J. E. Rocha, C. E. Souza, T. T. Yafawi, J. B. de Araújo Neto, F. F. Campina, J. C. Pinheiro, T. S. de Freitas, A. K. Sousa, S. R. Tintino, M. F. Braga, D. L. Vasconcelos, A. C. Barreto, J. H. da Silva, I. R. Menezes, R. N. Teixeira, J. C. Alvarez-Pizarro and H. D. Coutinho, "FTIR analysis and

reduction of the phytotoxic effect of mercury dichloride by rutin," *Rhizosphere,* vol. 19, p. 100393, 2021.

Chapter 5: Conclusions

5.1. Conclusion

The undoped and Au-doped V_2O_5 nanoparticles were successfully synthesised using the facile reflux method. The XRD analysis showed that the V_2O_5 nanoparticles had a shcherbianite orthorhombic crystal structure and the determined lattice parameters corresponding with those found in literature. The average crystallites sizes for undoped and Au-doped V_2O_5 increased at lower Au concentrations while decreased at higher Au concentrations due to an increased number of nucleation sites. SEM images exhibited the formation of nano-spherical nanostructure assembled by nanorods for undoped V_2O_5 and the decomposition of the nano-spheres to nanorods as the Au dopant was introduced. The nanorods were covered by thin nanowires due to the presence of Hg in the 2 wt% Au-doped V_2O_5 sample. The presence of the element Hg in the 2 wt% Au-doped V_2O_5 sample as a contaminant was also confirmed using the EDS. The BET results exhibited that all the prepared V_2O_5 nanoparticles were mesoporous materials with Type IV isotherm characteristics and the 2 wt% Au-doped V_2O_5 had the highest surface area of 30.67 m^2/g. The UV-Vis spectroscopy showed that the optical band gap of the prepared V_2O_5 nanoparticles increased with an increase in the concentration of Au, however, the 2 wt% Au-doped V_2O_5 sample band gap decrease due to the presence of Hg. The functional groups present in V_2O_5 were analysed using the FTIR spectroscopy.

Chapter 6: Recommendations, Limitations of study, Conferences and Future Work

6.1. Conference Presentations

6.3.1. Mokwena MM, Nubi OO and Akande AA, Synthesis and characterisation of Au-doped V_2O_5 nanostructures proposal, South African Institute of Physics (SAIP), 65th annual conference, North-West university, Potchefsroom campus, South Africa, 2021

6.3.2. Mokwena MM, Nubi OO and Akande AA, The effect of gold (Au) doping on the structural and optical properties of V_2O_5 nanostructures using the reflux method, Faculty of Science and agriculture research day (FSA-RD), 12th annual conference, Bolivia lodge, Polokwane, South Africa 2022

6.3.3 Mokwena MM, Nubi OO and Akande AA, Vanadium pentoxide (V_2O_5) nanostructures for gas sensing: doping and low-temperature detection of methanol, ethanol and NO_2 with superior response towards H_2S gas, South African Institute of Physics (SAIP), 67th annual conference, University of Zululand, Richards Bay campus, South Africa, 2023.

6.2. Limitations of the Study

This study was hindered by having limited resources (funds, facilities, and proper equipment) which partially prevented some of the objectives from being met. The undoped V_2O_5 and Au-doped V_2O_5 samples couldn't be tested for their gas detection properties due to time constraints. Comparing the results for the undoped sample with those of the Au-doped samples could have given more information on the effect of Au doping on the V_2O_5 sensing capabilities. The synthesis of the undoped and Au-doped V_2O_5 samples was done using the reflux method due to having no other alternative high-quality equipment to avoid contamination of samples.

6.3. Future Work and Recommendations

The main purpose of this work was to synthesise undoped and Au-doped V_2O_5 samples to be tested for the effect of Au concentrations on the structural, optical, and gas detection properties at low operating temperatures using a simple reflux method. Further characterisation of the undoped and Au-doped V_2O_5 samples to determine the oxidation state and binding energies of the elements composed in the prepared samples using X-ray photoelectron spectroscopy (XPS). The defects and lattice vacancies which affect the electronic band structure of a material induced during synthesis of samples can be revealed using the photoluminescence spectroscopy (PL). The fabrication of harmful gas and vapour sensitive MOS materials with high selectivity at low operating temperatures remain a challenge in gas detection research. In future the gas sensing properties of the refluxed Au-doped V_2O_5 samples towards various gases will further validate the applicability of the samples in society to reduce harm caused by air pollution. The use of capping reagents such as polyvinylpyrrolidine (PVP), ethylene diamine tetra acetic acid (EDTA), chitosan and more, can reduce the agglomeration of nanoparticles at higher concentrations of Au precursor to maintain the porous structure of the nanoparticles. The gas sensing properties of the Au-doped V_2O_5 nanoparticles will be studied to determine the selectivity and response towards various gases.